THE ASSESSMENT OF GAMMA HEATING IN REACTOR MATERIALS THROUGH DOSE AND TEMPERATURE MEASUREMENTS

By
M. L. DHAWAN

NUCLEAR ENGINEERING AND TECHNOLOGY PROGRAMME
INDIAN INSTITUTE OF TECHNOLOGY KANPUR
MAY, 1978

THE ASSESSMENT OF GAMMA HEATING IN REACTOR MATERIALS THROUGH DOSE AND TEMPERATURE MEASUREMENTS

A Thesis Submitted
In Partial Fulfilment of the Requirements
for the Degree of
MASTER OF TECHNOLOGY

By
M. L. DHAWAN

to the

NUCLEAR ENGINEERING AND TECHNOLOGY PROGRAMME
INDIAN INSTITUTE OF TECHNOLOGY KANPUR
MAY, 1978

NETP-1978-M-DHA-ASS

CERTIFICATE

Certified that the present work, entitled "The Assessment of Gamma Heating in Reactor Materials Through Dose and Temperature Measurements", has been carried out by Shri M.L. DHAWAN under my supervision and has not been submitted elsewhere for the award of a degree.

Rakesh Chawla

R. CHAWLA
Assistant Professor
Nuclear Engineering and Technology Programme
Indian Institute of Technology
KANPUR

May, 1978

ACKNOWLEDGEMENTS

First and foremost, I would like to express my sincere gratitude to Dr. R. Chawla for his efficient support, competent guidance and constant encouragement at all stages of this work.

I am very grateful for my sponsorship by the Bhabha Atomic Research Centre for doing my M.Tech. at I.I.T. Kanpur. I wish to express my heartiest thanks to Shri S.K. Mehta, Head RED, and Shri A. Kakodkar, Head CDAS/RED, for their encouragement, inspiration and assistance in carrying out the bulk of the experimental work for this thesis at BARC.

I am also indebted to Dr. C.M. Sunta of HPD, BARC, for several extremely useful discussions as well as for supplying the TLD powders and providing various facilities. Thanks are due to Dr. D.R. Bongirwar of FIPLY, BARC for his generous help and advice in carrying out the ^{60}Co irradiations. It is a pleasure to thank Dr. U.C. Gupta of DRP, BARC for assistance in the TLD calibrations.

I take the opportunity to express my thanks to Shri K.V. Kamath of RED, BARC, for the fabrication of various plates, to Shri N.C. Jain of RED for providing

thermocouple instruments, to Shri T.V. Kori of R-5 for his excellent tracings, to Shri J.D. Varma of I.I.T. Kanpur for elegant typing, and to Shri R.S. Tripathi for the cyclostyling.

Finally, the encouragement and inspiration given by my wife KRISHNA, is gratefully acknowledged.

M.L. DHAWAN

CONTENTS

LIST OF TABLES

LIST OF FIGURES

LIST OF PLATES

ABSTRACT

The use of thermoluminescent dosimeters (CaF_2 and LiF) for the determination of gamma-heating in reactor materials has been assessed in the light of temperature measurements across certain specially designed experimental assemblies. A 40 KCi ^{60}Co source was used for irradiation. The transport-theory code, ANISN, was employed for estimating gamma-spectra within the assemblies to enable the application of general cavity-ionization theory for the deduction of gamma-heating rates from TLD measurements. The measured heat-generation rates were fed as input to a three-dimensional heat conduction code, HEATING, to obtain various temperature drops across each assembly. These were compared with actual thermocouple measurements, reasonable agreement being obtained in each case.

CHAPTER 1

INTRODUCTION

In the design of nuclear power reactors, knowledge of gamma-ray heating effects is needed both for determining the cooling requirements for the reactor components and for predicting where thermal stresses will be important. If core, blanket and control-rod cooling requirements are to be correctly assessed ard optimum shielding specified in the design of a fast reactor, it is necessary to be able to determine the amount of energy that will be deposited by gamma-ray interactions in the various regions Gamma-ray heating measurements in zero-power criticals allow one to determine the adequacy of calculational techniques and gamma-ray-production cross-section libraries. They also provide gamma-ray heating profiles for a particular design and for regions not amenable to calculation.

A number of devices have been developed for gamma-ray dosimetry, e.g. cavity-ionization chambers, scintillation detectors, chemical dosimeters, solid-state integrating dosimeters, photographic emulsions and calorimeters. However, the particular environment of a reactor and other operational considerations limit the choice that one has. Measurements have to

be made in a mixed neutron/gamma radiation field in moderate fluences and in a variety of materials. It is also often necessary to perform simultaneous measurements in a number of different locations with probes that introduce minimum amount of perturbation. The thermoluminescent dosimeter (TLD) has proved to be the most suitable choice for gamma-ray heating measurements. TLD materials and techniques have developed over the last decade or so to an extent whereby a variety of dosimeters have become available for application to a wide range of exposure conditions.

There are two special areas of concern in the application of TLD techniques to the measurement of gamma-ray heating in reactors, viz. (i) the relationship between the energy deposited by gammas in the dosimeter and the heating in the surrounding medium, and (ii) the neutron sensitivity of the TLD material. The first effect is a function of the composition of the TLD and the surrounding material, the size of the TLD and the gamma-ray energy spectrum at the location under consideration. Since the gamma spectrum is not generally known accurately and since TLD materials are usually quite different from the materials in which gamma-heating measurements are to be made, it is important to choose the TLD suitably so as to minimize the uncertainty. As regards the second aspect, all TLD materials exhibit some response to

neutrons since ion recoils from elastic scattering, as well as gammas and/or other reaction-products from neutron capture, can cause ionization in the TLD material. Neutron-induced contributions to the TLD response must therefore be suitably corrected for in experimental gamma-heating studies in reactors.

In the present work, the adequacy of gamma-heating measurements made with CaF_2 and LiF TLD's has been directly assessed in the light of temperature measurements made using thermocouples. Special experimental assemblies were designed to enable such an assessment-steel, aluminium lead and teak wood being the materials considered. A pure gamma field provided by a 40 KCi cobalt-60 source was employed for the present study, the energy absorbed by the TLD's being related to the energy deposited in the surrounding material through the application of general cavity ionization theory. The latter required an estimation of the gamma-energy spectra at different location within each experimental assembly, and these were obtained from multigroup one-dimensional photon transport calculations using the ANISN code. With gamma-heating rates at different locations in a given assembly thus estimated from TLD measurements, a three-dimensional heat-conduction calculation was carried out using the code HEATING to obtain steady-state temperature drops across certain

specific locations. These calculated temperature drops were compared with actual thermocouple measurements made by irradiating the assembly for a period long enough to achieve steady-state temperatures.

Chapter 2 gives a general review of TLD principles and earlier applications. The present approach and design of experiments is discussed in Chapter 3, which also describes the analytical methods used, viz. the ANISN and HEATING codes. Particulars of the various experimental facilities and equipment used in the present study are given in Chapter 4. Results are presented and discussed in Chapter 5, while the final Chapter summarizes the conclusions and indicates the scope for further work.

CHAPTER 2

GENERAL REVIEW

Thermoluminescent dosimeters (TLD's) provide a useful means for measuring gamma-ray heating in critical facilities and shielding materials because of their high sensitivity, small size, easy handling, broad dose-measurement range, low neutron sensitivity, advanced state of development and adequate reproducibility/accuracy. This chapter gives a general review of TLD applications in reactor engineering.

2.1 TLD PRINCIPLES

The basic principle of the TLD is quite simple. The thermoluminescent (TL) material contains a number of electron or hole traps, stable at room temperature. An ionizing particle in passing through the material raises electrons into the conduction band and some of these electrons, instead of falling directly back to the ground state, are captured in trapping centres at some intermediate energy level. A trapped electron cannot get to a lower energy state except by first returning to the conduction band. When the material is heated to approximately 300 ^{o}C, the electron (or hole) is released from the trapping centre by thermal ionization and moves through the crystal until electron-hole annihilation takes place at a recombination centre. During

this process thermoluminescent emission occurs which can be detected by a photomultiplier tube. The number of photons released, and thus the intensity, are related to the material's exposure. Figure 2.1 (a) depicts the trapping of an electron/hole during exposure, while Fig. 2.1 (b) depicts the emission of the TL photon on heating.

2.2 SUMMARY OF EARLIER APPLICATIONS

Extensive developments in TL materials and techniques during the last ten years have resulted in dosimeters that are applicable to a wide range of exposure conditions and are being increasingly employed for personnel dosimetry (1, 2) . TLD techniques have also been applied to reactor studies (as discussed below) and to other mixed radiation environments such as those encountered in weapons testing. For gamma-heating measurements with CaF_2 : Mn dosimeters in various reactor materials, the dose/response relationship may be determined with an accuracy of typically 3%, while for LiF errors are generally larger because of the greater energy dependence.

Calorimetric measurements of gamma-ray heating rates in critical assemblies are very difficult, since the gamma flux at a typical power level of 50 - 100 watts would cause a temperature rise of only about

10^{-3} °C/hr, assuming perfect insulation of the calorimeter. Consequently, the possibility of indirect measurements was considered, and it was concluded that an ionization detector would provide the desired information with the requisite sensitivity. The TLD was chosen, in preference to ionization chambers, because of the inherently smaller probe size and the possibility of making simultaneous measurements at a number of different positions. Photographic emulsions were also considered in the early stages, but TLD's were soon recognised as being considerably more advantageous.

Stanford and Johnson (3) used CaF_2 : Mn powder to measure gamma-ray heating in a thermal critical facility. Measurements were made in the vicinity of the core at operating powers of 20 - 300 watts. The Bragg - Gray principle of cavity ionization (Sec. 2.3) was used in analyzing the data, experimentally determined corrections being applied to account for the gamma-ray spectral effect and neutron sensitivity. The reproducibility of the measurements was typically about 5 - 10%. Absolute results were subject to an additional uncertainty of ± 15% in the determination of the reactor power.

Adamson, et. al. (4) used LiF powder to measure gamma-ray heating as a function of position within a single lattice cell at the centre of ZEBRA-6,

a zero-power fast reactor assembly. Boulette and Bunch (5) used LiF ribbons (3 x 3 x 0.9 mm) for checking the shield design of the Fast Flux Test Reactor (FFTR). In further support of the FFTR programme, Stanford, et al (6) exposed ^{7}LiF rods (1 x 1 x 6 mm) in the ZPR-9 critical assembly. LiF TLD's were also used for dose mappings, single-cell dose heterogeneity and blanket-reflector and reflector-core interface studies for the Experimental Breeder Reactor (EBR - II) series of ZPR - 3 critical assemblies (7).

Absolute gamma-ray heating was investigated by Simons and Olson (8) in Assembly-2 of the Zero Power Plutonium Reactor (ZPPR). The first series of experiments was devoted to obtaining axial and radial absorbed-dose maps for the LMFBR Demonstration Benchmark Critical. The second and third series of experiments determined the heating measurements inside LMFBR control-rod assemblies. All measurements were made with ^{7}LiF TLD's (enriched to 99.993% ^{7}Li) encapsulated in stainless steel. Fast-neutron spectra were measured inside the plutonium - fuelled critical assembly near the centre of the inner and outer core zones by proton-recoil proportional counters, and also calculated by the DOT code. (All neutron cross-sections needed for the DOT code were obtained from library tapes prepared using MC^{2}, CALHET

and CCXS). The gamma-ray source in a given photon group due to neutron induced gamma-ray-production reactions was calculated by the POPOP4 code. Finally, using Compton - effect, photoelectric and pair production cross-sections from a MUG library tape, absorbed - gamma doses were calculated in rads/sec from the relation

$$D = C \sum_{J=1}^{N} \left[\phi_J \left(E_{av} \frac{\mu_{en}}{\rho} \right)_J \right]$$

where C is the conversion factor 1.602×10^{-8} gm/Mev

ϕ_J is the photon flux in the Jth group (J = 1, ...,N), in photons/cm^2 - sec

$(E_{av})_J$ is the average photon energy of the Jth group, in Mev

$\left(\frac{\mu_{en}}{\rho}\right)_J$ is the mass energy absorption coefficient of the material for gamma-energy E_{av}, in cm^2/gm.

Excellent agreement was obtained between calculated absorbed doses and results of measurements with ^{7}LiF TLD's.

It should be mentioned that a few calorimetric measurements of gamma - ray heating in fast reactors have also been recently reported, e.g., by Price, Laskiewicz and Lowery (9) and by Reilly and Peters(10) . Two different types of calorimeters were used - an active calorimeter using thermocouples, and a passive calori-meter termed as the gamma expansion difference monitor

(GEDM). The latter system employed thermal expansion difference (TED) monitors, each consisting of a small cylindrical stainless steel capsule completely filled with sodium.

Another type of TLD application in reactor engineering, i.e. apart from gamma-heating measurements, has been the determination of in-core thermal-neutron fluxes (11), LiF crystals enriched with either ^{6}Li or ^{7}Li allowing the application of two alternative neutron/gamma discrimination techniques. In the first method, both types of crystals were employed. The ^{6}LiF (95.62% ^{6}Li) dosimeters, due to the large thermal neutron cross-section for ^{6}Li, detected both neutrons and gamma radiation, while ^{7}LiF (99.993% ^{7}Li) dosimeters, possessing negligible thermal-neutron attenuation characteristics, monitored the gamma component only. The dosimeters were inserted into the reactor for a known time and read on a commercially available detection system, the difference in the response of the two types of dosimeters yielding a direct measure of neutron flux. The second technique used bare and cadmium-covered ^{7}LiF dosimeters. The bare crystals detected reactor gammas, while those encapsulated in cadmium measured reactor gammas plus capture gammas from the ^{113}Cd (n, γ) reaction. The difference in response provided the capture-gamma contribution, which was proportional to the neutron flux.

2.3 CAVITY-IONIZATION THEORY

When a dosimeter, e.g. an ionization chamber or TLD, is introduced into a medium for measurement of dose, the energy absorbed per unit mass in the medium is usually different from that absorbed by the dosimeter since the dosimeter and surrounding medium are generally different materials. Cavity ionization theory (12) provides the relationship between the energy absorbed per unit mass in the medium, E_m, and that in the dosimeter, E_D, in the form

$$E_m = \frac{1}{f} E_D \qquad (2.1)$$

where f is, in general, a function of the (a) gamma ray-energy, (b) composition of the surrounding medium, (c) composition of the TLD material and (d) size of the dosimeter.

A simple theory of cavity ionization results if one assumes the following:

(i) The primary electrons created by photon interactions lose their energy continuously.

(ii) The cavity does not perturb the equilibrium electron energy distribution established in the medium, and

(iii) Photon interactions in the cavity material are negligible.

The latter two assumptions imply that the size of the cavity is small compared to the electron ranges in the cavity material. If one primary electron is generated per unit mass of the medium with energy T_o, and if electron equilibrium exists, the energy absorbed per unit mass of the medium is T_o. The energy deposited in the cavity is

$$\int_o^{T_o} N_m (T_o, T) \left(\frac{1}{\rho} \frac{dT}{dx} \right)_D dT \qquad (2.2)$$

where $N_m (T_o, T)$ is the electron slowing-down energy distribution characteristic of the medium and, according to assumption (1), is the reciprocal of the mass stopping power of the medium. $\left(\frac{1}{\rho} \frac{dT}{dx} \right)_D$ is the mass stopping power for the cavity material. The energy dissipated per unit mass of the dosimeter material divided by the energy dissipated per unit mass of the medium is given by

$$f_s (T_o) = \frac{1}{T_o} \int_o^{T_o} \frac{\left(\frac{1}{\rho} \frac{dT}{dx} \right)_D}{\left(\frac{1}{\rho} \frac{dT}{dx} \right)_m} dT \qquad (2.3)$$

If the energy dependence of the mass stopping powers is neglected, the above equation reduces to the well known Bragg - Gray relationship. To determine $f_s (T_\gamma)$, the f_s value associated with a given monoenergetic gamma-ray of energy T_γ, [illegible] averaging over the three

primary electron spectrum components produced by the gamma-ray is carried out, giving

$$f_s(T_\gamma) = F_p(T_\gamma)\,{}_pf_s + F_c(T_\gamma)\,{}_cf_s + F_{pp}(T_\gamma)\,{}_{pp}f_s \qquad (2.4)$$

where the subscripts p, c and pp denote photoelectric, Compton and pair production interactions respectively, F_i is the interaction probability and ${}_if_s$, the corresponding f_s term.

The small-cavity assumptions made above are not valid for typically sized solid-state dosimeters exposed in reactor gamma-ray spectra. The electron spectrum in the cavity is not identical to that in the medium, and the effect of gamma-ray interactions with cavity material is not negligible. In the limit of a large cavity (the range of the most energetic electrons is small compared to the cavity dimensions), the energy deposited in the cavity is simply

$$E_D = N\,T_\gamma \left(\frac{\mu_{en}}{\rho}\right)_D \qquad (2.5)$$

where N = gamma-ray fluence

T_γ = gamma-ray energy

$\left(\frac{\mu_{en}}{\rho}\right)_D$ = the mass absorption coefficient for the dosimeter material.

A similar expression holds for the surrounding medium. Thus in the large-cavity limit, the energy absorbed per unit mass of the dosimeter material divided by the energy absorbed per unit mass of the medium is given by

$$f_1(T_\gamma) = \frac{\left(\frac{\mu_{en}}{\rho}\right)_D}{\left(\frac{\mu_{en}}{\rho}\right)_m} \qquad (2.6)$$

A comprehensive theory of cavity ionization must reduce to the small-cavity result at large electron ranges and to the large-cavity result at small electron ranges. Burlin (13) proposed an approximate method of solving the general problem by considering that the presence of the cavity in the medium modifies the electron spectrum in two ways, viz.

(i) the electron spectrum generated by the photons in the medium and emitted from the wall of the cavity will be partially or completely absorbed as it crosses the cavity and

(ii) the photons will generate in the cavity an electron spectrum which will build up and possibly reach equilibrium at increasing distances from the cavity wall.

To a first approximation, it may be said that the electrons are attenuated exponentially without any change in

the spectral distribution, the effective mass absorption coefficients being assumed the same for the "wall spectrum" and the "cavity spectrum". Thus the electron spectrum in the cavity at a distance x from the wall is reduced by the factor $e^{-\beta x}$, and the electron spectrum generated in the cavity will have risen to $(1 - e^{-\beta x})$ of its equilibrium value. β is the *effective mass absorption coefficient* and for the case of interacting gamma-rays of energy T_γ, is given by

$$\beta = \frac{16}{(T_\gamma - 0.036)^{1.40}} \quad cm^2/gm \qquad (2.7)$$

g, the average path length of electrons crossing the cavity, is given by

$$g = \frac{4V}{S} \qquad (2.8)$$

where V is the volume and S is the surface area of the dosimeter. Then, on average, the wall spectrum will be reduced by a factor

$$\frac{\int_0^g e^{-\beta x}\, dx}{\int_0^g dx} = \frac{1 - e^{-\beta g}}{\beta g} = d \qquad (2.9)$$

The cavity spectrum will build up to a fraction of its equilibrium value given by

$$\frac{\int_0^g (1 - e^{-\beta x})\, dx}{\int_0^g dx} = \frac{\beta g + e^{-\beta g} - 1}{\beta g} = (1 - d) \qquad (2.10)$$

The energy absorbed per unit mass of the desimeter material divided by the energy absorbed per unit mass of the surrounding medium may finally be approximated by

$$f(T_\gamma) = d\, f_s(T_\gamma) + (1 - d)\, f_l(T_\gamma) \qquad (2.11)$$

Equation (2.11), the general-cavity theory result, reduces to equation (2.3) for the case of a small cavity ($g \to 0$, $d = 1$) and to equation (2.6) for a large cavity ($g \to \infty$, $d = 0$). This general result forms the basis for carrying out gamma-heating measurements. For an incident gamma spectrum described over N energy groups, i.e. ϕ_i, $i = 1, 2, \ldots N$, the effective $\frac{1}{f}$-factor to be used for converting the TLD dose to energy absorption in the medium would be

$$\frac{1}{f} = \frac{\underset{i}{\text{Sum}} \left(\frac{1}{f_i} \cdot \phi_i\right)}{\underset{i}{\text{Sum}}(\phi_i)} \qquad (2.12)$$

where f_i is evaluated at the mean gamma energy for the ith group.

2.4 FACTORS EFFECTING RESPONSE-DOSE RELATIONSHIP FOR TLD'S

A TLD is not an absolute radiation detector. It is thus necessary to determine empirically the relationship between the TL response and the energy deposited in the dosimeter by exposures in known fields

of radiation. The relationship between the TL response and E_D may be a function of several variables such as the TLD material, the dose, the dose rate, the energy of the gamma-rays which produced the dose, the heating rate, the time between the irradiation and readout, environmental factors before, during and after the irradiation, and the pre- and post-annealing history of the dosimeter.

The dose-response curve of CaF_2 : Mn is linear up to the point at which saturation occurs. LiF exhibits a supralinear behaviour beginning at about 10^3 rads, below which the response is linear (2).

The energy response is the dependence of the dose/response curve on the energy of the gamma-rays which produce a given dose. For CaF_2 : Mn, the response per rad appears to be independent of the gamma-ray energy, whereas for LiF there are certain finite radiation - quality dependent effects in the TL response at low electron energies.

Both LiF and CaF_2 : Mn show evidence of fading. The amount of fading is less than 10% per month and appears to follow an exponential behaviour. If all the dosimeters used in a particular experiment are always read out at a fixed time after irradiation, corrections for fading effects become unnecessary.

The LiF response is somewhat more sensitive to the dosimeter's past history than is the CaF_2 : Mn response. The response of LiF significantly decreases if the phosphor has been exposed previously to radiation greater than 10^4 rads. This difficulty can be overcome if the calibration of the dosimeter is carried out from the same batch. With commercially available readout devices and dosimeters, it is possible to obtain 2 to 3% reproducibility for a given dosimeter, as well as, from dosimeter to dosimeter within the same batch.

2.5 NEUTRON SENSITIVITY

When carrying out gamma-heating measurements in a reactor environment, the sensitivity of the TLD response to fast and thermal neutrons has to be assessed and corrected for if necessary.

Thermal neutrons create ionization in the material either through charged-particle reactions, such as $^6Li\ (n, \alpha)\ ^3H$ in a LiF dosimeter, or through gamma-producing reactions, such as $^{25}Mn\ (n, \gamma)\ Mn^{26}$ in CaF_2 : Mn dosimeters. For gamma-ray heating determination in a thermal reactor environment, the CaF_2 : Mn dosimeter is preferable because it shows minimal sensitivity to neutrons (14). The sensitivity of various TLD's to thermal neutrons has been reported by Busuoli and Cavallini (15) and is reproduced below:

Material	Response/10^{10} cm^{-2} (relative to response/R of ^{60}Co gamma-rays)
LiF (TLD-600)	1930
LiF (TLD-100)	350
$Li_2 B_4 O_7$: Mn	310
LiF (TLD-700)	1.5
CaF_2 : Mn	0.6
$CaSO_4$: Dy	0.5
BeO	0.3

TLD's exhibit a thermoluminescent response to fast neutrons. The elastic scattering of fast neutrons by the lattice ions produces ion recoils. The slowing down of these recoils creates electron-hole pairs, which may then become trapped. The slowing down also leads to the production of defects - ions are displaced, and in a multicomponent system replacement collisions also take place. Beside the contribution to the fast-neutron response associated with the production of electron-hole pairs, the TL output may also be affected by the production of lattice-ion displacements and lattice vibrations. A neutron-erasing effect has been reported for LiF TLD phosphor (16). Fast neutrons seemed to have the effect of removing electrons from their traps, thereby erasing some of the stored information, but Stanford and Johnson (3)

observed no significant indication of a neutron-erasing effect during their experiments. Goldstein, et al. (17) have found that for fast-neutron fluences as high as 10^{15} n/cm^2, the gamma-ray and fast neutron responses are additive, so that even though there are a sizable number of defects introduced, the TL output is not significantly affected. The fast-neutron-associated contribution to ^{7}LiF TL response was estimated by Simons and Yule (18) to be typically 10% in a fast-reactor environment. Such contributions would obviously be different for different TLD materials. Puite (19) has reported that no permanent change in TL sensitivity for gamma-rays is observed after fast-neutron irradiations of upto 8 x 10^{13} n/cm^2.

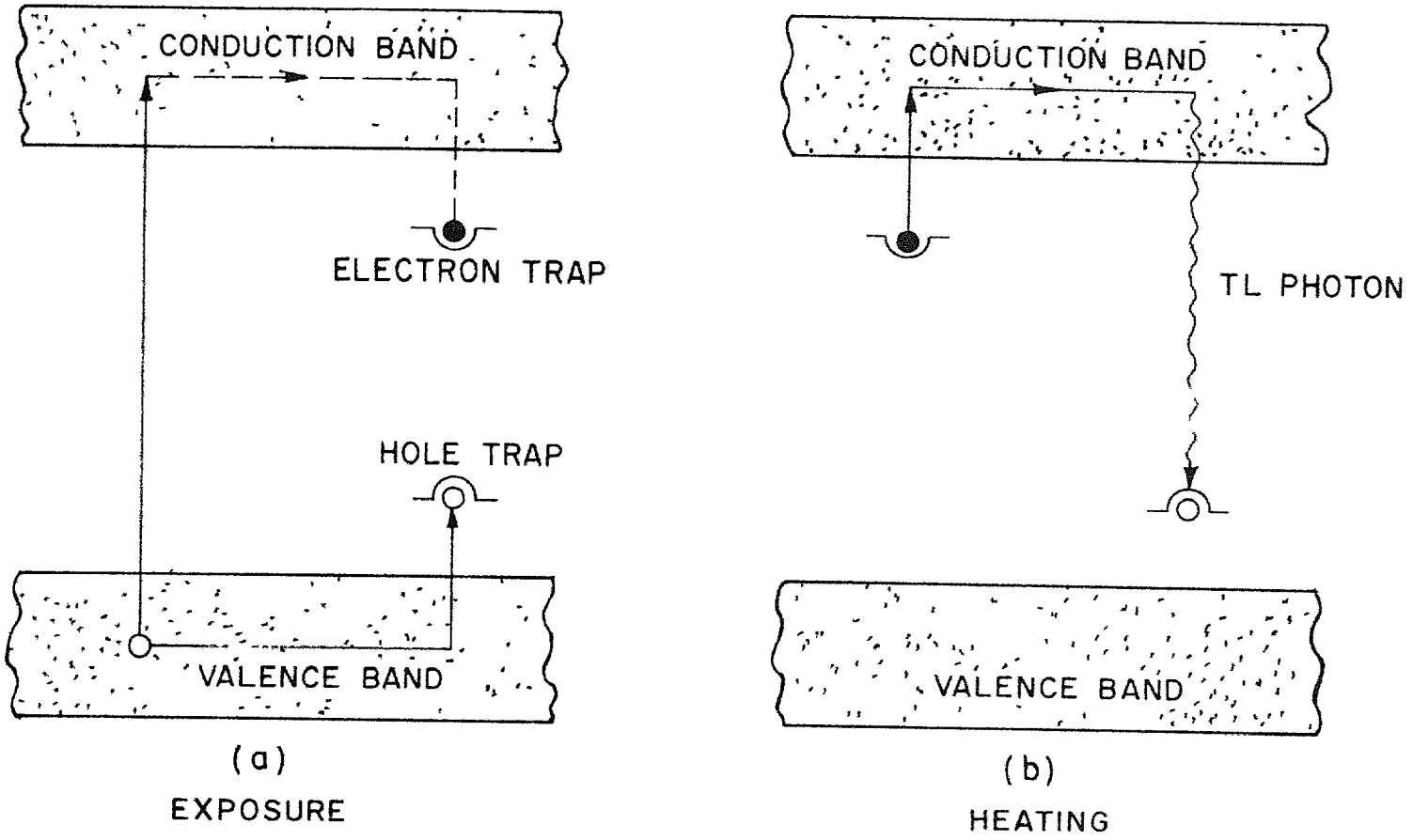

FIG 2 | TLD PRINCIPLE

CHAPTER 3

PRESENT APPROACH AND ANALYTICAL METHODS USED

3.1 DESIGN OF EXPERIMENTS

From the review of earlier gamma-heating measurements given in Section 2.2, it is seen that temperature rises associated with radiation heating experiments in facilities such as low-power research reactors usually amount to very much less than a degree, necessitating the use of TLD's for deduction of energy deposition rates. Calorimetric methods involving temperature measurements are generally not applicable. The present work has involved the design of certain experiments to enable results of gamma-heating measurements made using TLD's to be directly assessed in the light of temperature measurements made using thermocouples.

It was felt that for establishing the feasibility of such comparisons, a pure gamma - field provided by a strong cobalt - 60 source would be adequate. Accordingly, the FIPLY*facility at B.A.R.C. (Section 4.1) which provides a planar cobalt - 60 source of $\simeq$ 40 KCi strength, was chosen for the present study. At the irradiation position available ($\simeq$ 20 cms from the plane of the source), the gamma flux was $\simeq 10^{12}$ cm^{-2} sec^{-1}, which is typical of that available with low-power reactors.

---

*Food Irradiation & Processing Laboratory

If one considers, for example, a 5 cm thick steel slab exposed to the above gamma flux, the order of magnitude of the steady - state temperature drop across the slab would be $\simeq 2 \times 10^{-2}$ °C. This low value, of course, results from the high thermal conductivity of steel. The approach presently taken has been to use materials of low thermal conductivity in conjunction with materials of high thermal conductivity to obtain measurable temperature drops. Thus, to extend the above simple example of a 5 cm steel slab, consider this surrounded by 5 cm thick slabs of wood (a material often employed for neutron shielding). The steady - state temperature drop across the wood would be as high as $\sim$ 20 °C, if one assumes that all the heat generated in the steel is conducted through the wood. The gamma - heating in the high - conductivity steel thus gets reflected in an easily measurable temperature drop across the low-conductivity wood.

In actual practice, due to heat conduction through the steel in the Y and Z directions (taking X as the thickness direction), this temperature rise would not be obtained. However, if insulating material is provided in the Y and Z directions, so that most of the heat is in fact conducted through the wood, a measurable temperature drop would certainly be registered. In the present work, 4 - 8 cm of thermocole

was used for providing the necessary insulation for the experimental assemblies in the Y, Z directions (Sec. 4.2).

A comparison of results for temperature differences deduced from dose measurements with actual thermocouple measurements would involve an accurate heat - conduction calculation in the X, Y, Z direction. The 3 - dimensional code, HEATING, was used for the purpose and this is described in Section 3.3.

For obtaining energy deposition (heat generation) rates at different locations in a given experimental assembly using TLD's, it is essential to estimate the gamma - energy spectrum at the various points (Sec. 2.3). This was presently done by conducting one-dimensional photon transport calculations using the ANISN code (Sec. 3.2).

While carrying out the temperature measurements, relatively long irradiations would be necessary for achieving steady - state conditions. With the FIPLY gamma - flux indicated earlier TLD irradiations, on the other hand, would have to be for typically $\leq$ 2 mins. to avoid saturation in the response. For such short irradiations the effects of transient dose, received while bringing the source into position and while removing it, must be accurately corrected for. Thus, in

the present case, the FIPLY source was located under 18 ft of water when not in use. For carrying out an irradiation the source was raised into position, an operation that took about 45 seconds during which significant doses were recorded by the TLD's. Similarly, at the end of the irradiation, a transient dose was recorded while lowering the source. Since gamma - heating rates had to be assessed in terms of watts per sec. of steady exposure, it was essential to carry out two sets of TLD measurements (for, say, 1 and 2 minutes of steady exposure) - so that the effects of the transients could be corrected for.

3.2 ANISN CODE

ANISN is a one-dimensional, discrete-ordinates transport code and solves the one-dimensional, energy - dependent Boltzmann transport equation with anisotropic scattering for slab, cylindrical and spherical geometries (20, 21). ANISN solves forward or adjoint, homogeneous or inhomogeneous, neutronic or photonic problems. The inhomogeneous problems may have a fixed-volume, distributed source or a specified angular - dependent shell source at any mesh interval. Fissions may be included for a subcritical system. Vacuum, reflective, periodic, white or albedo boundary conditions

may be specified. Cross-sections may be input from a library tape and/or from cards. Fixed distributed sources or shell sources may be input from cards and/or from tape. The code also includes space-point scaling to accelerate the flux solution on inner iterations.

The discrete-ordinates, or Carlson's (22) S_n, method using a diamond - difference solution technique is employed. The solution in the code will approach the exact solution of the Boltzmann equation with increasing orders of approximations as the space, angle and energy meshes approach differential size.

The input data for the ANISN code are divided into the following five data sets:

(A) Overall problem parameters

(B) Cross-section data

(C) Fixed-source data

(D) Flux or fission guess data

(E) Remainder of data.

A discussion of (B), the cross-section data, is pertinent here. ANISN expects a table of cross-sections for each energy group, g, for each material in the following format:

Position	Cross-section type	
1	σactivity	Optional
2	σactivity	
.	.	
.	.	
.	.	
IHT-2	σabsorption	
IHT-1	σfission	
IHT	σtotal	
IHT+1	$\sigma_{g,\ +\ NUS^* \rightarrow g}$	Upscatter
.	.	
.	.	
.	.	
IHS-1	$\sigma_{g\ +\ 1 \rightarrow g}$	
IHS	$\sigma_{g \rightarrow g}$	Downscatter
IHS+1	$\sigma_{g-1 \rightarrow g}$	
.	.	
.	.	
.	.	
IHM	$\sigma_{g\ -\ NDS^* \rightarrow g}$	

Activities may be computed by zone and interval. This option provides a rapid and economical way to obtain data such as reaction rates, dose rates, capture or other desired response rates. For the type of photonic calculations presently conducted (pair - production events negligible),

$\sigma_{absorption} = \tau$ (the photoelectric cross-sections)

$\sigma_{total} = \tau + \sigma$ (the sum of photoelectric and Compton cross-sections)

These values can be obtained from standard handbooks (23) at different gamma-energies.

For the scattering cross-sections, with only down scatter possible, $\sigma_{g \to g'}$ $(g' > g)$ values are obtained from the Klein - Nishina equation (24). The equation is

$$\frac{d\sigma_c^{KN}}{d\Omega} = \frac{r_o^2}{2}\left[1 + \alpha(1 - \cos\theta)\right]^{-2} \cdot \left[1 + \cos^2\theta + \frac{\alpha^2(1 - \cos\theta)^2}{1 + \alpha(1 - \cos\theta)}\right] \text{ cm}^2/\text{electron-sterdian} \qquad (3.1)$$

where $\alpha = \frac{E_o}{0.511}$, $r_o = 2.82 \times 10^{-13}$ cm (classical radius of the electron)

and $\cos\theta = 1 + \frac{0.511}{E_o} - \frac{0.511}{E_1}$, E_o being the initial energy and E_1 the final energy after scattering through angle θ.

Now, $d\Omega = 2\pi \sin\theta \; d\theta$.

Putting $(1 - \cos\theta) = z$, so that $\sin\theta \, d\theta = dz$, and integrating Equation (3.1) from $z = 0$ to $z_1 = (1 - \cos\theta)$ we get

$$\sigma_c^{KN} = \pi \times 7.94 \times 0.603 \times 10^{-2} \frac{Z\rho}{A} \left[\left(\frac{1}{2\alpha} + \frac{2}{\alpha^2} \right) + \frac{1}{\alpha^3}(1+\alpha z_1) - \frac{1}{2\alpha(1+\alpha z_1)^2} - \frac{1}{(1+\alpha z_1)} \cdot \left(\frac{2}{\alpha^2} + \frac{1}{\alpha^3} \right) - \ln(1+\alpha z_1) \cdot \left(\frac{2}{\alpha^3} + \frac{2}{\alpha^2} - \frac{1}{\alpha} \right) \right] \text{cm}^{-1} \quad (3.2)$$

Consider, for example, a gamma-energy group structure with 1.4 - 1.1 Mev as the first group, 1.1 - 0.9 Mev as the second and so on (Section 5.2). In this case $\sigma_{1 \to 1}$ is got from Equation (3.2) by taking E_o = 1.25 Mev and E_1 = 1.1 Mev. For $\sigma_{1 \to 2}$, E_o = 1.25 Mev and E_1 = 0.9 Mev. The other $\sigma_{g \to g'}$ values appropriate to the given group structure are obtained in a similar manner.

3.3 HEATING CODE

The HEATING program is a generalized heat-conduction code with reasonably simplified input requirements (25, 26). The program establishes a network of nodal points throughout the specified configuration alongwith their relative locations and boundary conditions to enable the performing of nodal heat balances. The conductances from a given point to each of its neighbour points are calculated, and the program then computes the temperature distribution for transient and/or steady-state heat-conduction problems in one, two or

three dimensions using either cartesian or cylindrical polar co-ordinates.

The initial temperature pattern may be specified as a function of position. Boundary temperatures may be time-dependent and heat generation rates may be time - and/or position - dependent. HEATING offers nine possible geometries, which are members of cylindrical polar or rectangular co-ordinate systems, and three boundary types which are numbered 0, 1 or 2 corresponding to the following:

0 - same effect as a zero-numbered boundary

1 - convective heat transfer type

2 - controlled surface temperature type.

The spatial description of the problem is given in the form of mesh points/lines in each direction upto a maximum of 500.

The calculations are based on the assumption that the heat transfer within the material follows Fourier's Law of heat conduction. In cartesian co-ordinates, the conduction equation for steady-state conditions is

$$\frac{d}{dx}\left[K(x, y, z)\frac{dT}{dx}\right] + \frac{d}{dy}\left[K(x, y, z)\frac{dT}{dy}\right] + \frac{d}{dz}\left[K(x, y, z)\frac{dT}{dz}\right] + Q(x, y, z) = 0 \qquad (3.3)$$

where T is the temperature, K is the position-dependent thermal conductivity and Q is the position - dependent volumetric heat generation rate.

The boundary condition is

$$T_b = f(x, y, z) \tag{3.4}$$

$$\text{OR} \quad -K \left(\frac{dT}{dx} \right)_b = h \left[T_b - f(x, y, z) \right] \tag{3.5}$$

Consider a specified nodal point j which is thermally connected with M adjacent nodal points. By a heat balance on the node j, we get

$$\sum_{i=1}^{M} {}_jK_i (T_i - T_j) + Q_j = 0 \tag{3.6}$$

Similar equations are written for all the nodes. The value of T_j is obtained by iteration. Assume that the (n + 1)th iteration gives the correct value T_j^{n+1} and satisfies equation (3.6). The nth iteration value T_j^n gives a residual value E when substituted in equation (3.6), i.e.

$$\sum_{i=1}^{M} {}_jK_i (T_i - T_j^n) + Q_j = E \tag{3.7}$$

$$\text{Also,} \quad \sum_{i=1}^{M} {}_jK_i (T_i - T_j^{n+1}) + Q_j = 0 \tag{3.8}$$

From Equations (3.7) and (3.8)

$$E = \sum_{i=1}^{M} {}_jK_i \left(T_j^{n+1} - T_j^n \right) \tag{3.9}$$

Rewriting Eqn. (3.7), we get

$$\sum_{i=1}^{M} {}_{j}K_{i} \, (T_{i} - T_{j}^{n}) + Q_{j} = (T_{j}^{n+1} - T_{j}^{n}) \sum_{i=1}^{M} {}_{j}K_{i} \tag{3.10}$$

To increase the convergence rate, one uses $T_{i} = T_{i}^{n}$ for $i > j$ and $T_{i} = T_{i}^{n+1}$ for $i < j$. By using Equation (3.10) the temperature imbalance is brought to minimum at all nodal points. An over-relaxation of the imbalance can be done by multiplying the left hand side of Equation (3.10) by a parameter β , i.e.

$$\beta \left[\sum_{i=1}^{M} {}_{j}K_{i} \, (T_{i} - T_{j}^{n}) + Q_{j} \right] = (T_{j}^{n+1} - T_{j}^{n}) \sum_{i=1}^{M} {}_{j}K_{i} \tag{3.11}$$

Re-arranging the above equation

$$T_{j}^{n+1} = T_{j}^{n} \, (1 - \beta) + \beta \left(\frac{\sum_{i=1}^{M} {}_{j}K_{i} \, T_{i} + Q_{j}}{\sum_{i=1}^{M} {}_{j}K_{i}} \right) \tag{3.12}$$

Use of Equation (3.12) is known as the extrapolated Liebmann method. β must be in the range 1.0 - 2.0. The suggested optimum value of β is

$$\beta = 2 - 2 \left[1 - \left(\frac{T^{n+2} - T^{n+1}}{T^{n+1} - T^{n}} \right)^{1/2} \right]^{1/2} \tag{3.13}$$

Equation (3.12) is iterated, replacing T^{n} by T^{n+1}, until the maximum absolute value of $(T_{j}^{n} - T_{j}^{n+1})/(T_{j}^{n+1})$ is less than the specified convergence criterion, say 10^{-4}.

CHAPTER 4

EXPERIMENTAL PARTICULARS

The various experimental facilities used in the present work are described in this chapter.

4.1 FIPLY FACILITY

The cobalt-60 source employed for irradiation of the experimental assemblies was that of the FIPLY facility at the Bhabha Atomic Research Centre, Trombay. At the time of experimentation, the strength of the source was $\simeq 40$ KCi. A schematic diagram of the FIPLY facility is shown in Fig. 4.1. The source consists of 38 pencils in two racks as shown in Fig. 4.2 (a). Each pencil consists of a cluster of 5 cobalt-60 slugs (27), encapsulated in stainless steel as shown in Fig. 4.2 (b). On either side of the source, irradiation channels of 34 cm width and 26 cm height are provided (Fig. 4.1). The source room has staggered concrete shielding to minimize direct streaming and is separated from the control room by an interlocking door. Plate 1 gives a view of the FIPLY source room showing a "thermocouple assembly" (Sec. 4.2) being positioned in the irradiation channel. Plate 2 is a view of the control console in the FIPLY control room.

4.2 PLATES AND ASSEMBLIES

Plates (300 mm length, 150 mm width and of various thicknesses) of steel, aluminium, lead and wood (teak) were fabricated to a specified surface finish of 1.6 microns to ensure good thermal contact. Plate 3 shows the various types of experimental plates. From these plates, different assemblies were made with thermocole insulation on each side, of 40 mm thickness in the Y - direction and 80 mm in the Z - direction. The various dimensions were largely dictated by the space available in the FIPLY irradiation channel.

To enable dose measurements to be carried out, each plate in the "TLD assembly" was provided with nine 16 mm - diameter holes (5 mm deep for steel and lead, 8 mm for aluminium and 16 mm for wood). TLD - carrying blanks of the appropriate material and dimensions could be fitted in these holes. Plate 4 gives a view of the various types of blanks used. Plate 5 shows the partly assembled aluminium TLD assembly with thermocole insulation.

For carrying out temperature measurements, it was felt that for ease of experimentation, a separate set of assemblies be used. These were constructed from thicker plates than employed for the TLD assemblies

so as to minimise any finite effects due to air gaps. Two of the plates of each material (excluding wood) were provided with alumel-chromel thermocouples, spot-welded on the surface at the centre with the leads running along 2 mm deep slots. Table 4.1 summarises the configuration for each type of experimental assembly presently investigated.

TABLE 4.1 The Various Assemblies

No.	Assembly	Overall Thickness	Constituent Plates for TLD Assemblies	Constituent Plates for Thermocouple Assemblies
1.	Steel	160 mm	5 mm Al (25+25)mm W (6+6+6+6+6+10+10)mm S (25+25)mm W 5mm Al	*5 mm Al (25+25)mm W (*10+20+20*)mm S (25+25)mm W 5* mm Al
2.	Aluminium	210 mm	5 mm Al (25+25)mm W (10+10+10+10+20+20+20)mm Al (25+25) mm W 5 mm Al	*5 mm Al (25+25)mm W (*20+20+20+20+20*)mm Al (25+25)mm W 5* mm Al
3.	Lead	90 mm	5 mm Al (25+25) mm W (6+6+6+6+6) mm L (25+25) mm W 5 mm Al	*5 mm Al (25+25) mm W (*10+20*) mm L (25+25)mm W 5* mm Al
4.	Combination-1	220 mm	5 mm Al (25+25)mm W (10+10)mm S (25+25)mm W (10+10+10+10)mm Al (25+25)mm W 5mm Al	*5 mm Al (25+25)mm W (*20*)mm S (25+25)mm W (*20+20*)mm Al (25+25)mm W 5*mm Al
5.	Combination-2	220 mm	5mm Al (25+25)mm W (10+10+10+10)mm Al (25+25)mm W (10+10)mm S (25+25)mm W 5mm Al	*5 mm Al (25+25)mm W (*20+20*) mm Al (25+25)mm W (*20*) mm S (25+25)mm W 5* mm Al

In Table 4.1, *' indicates a thermocouple mounted on the plate and Al, W, S and L denote Aluminium, Wood, Steel and Lead respectively.

4.3 TLD'S AND TLD CALIBRATION FACILITY

Pure CaF_2 and LiF powders prepared by the Health Physics Division, B.A.R.C., were the TLD's used. The parallel use of both these types of TLD was meant to provide a check on any possible systematic errors in calculating $\frac{1}{f}$ - factors.

If a dosimeter is to be used for absolute measurements, it must be calibrated in a known radiation field. During the calibration, as during the dose measurements, the TLD must be enclosed in a capsule of suitable thickness to establish electronic equilibrium (2). For cobalt-60 radiations (mean energy, 1.25 Mev), the amount of "build-up" material required is about $0.45/\rho$ cm., where ρ is the density of the capsule material in gm/cm^3. The build-up required for the various types of blanks used is compared in Table 4.2 with the build-up actually provided.

TABLE 4.2 Build-up required and provided in TLD Blanks

Blank	Build-up required	Build-up provided
Steel	0.57 mm	1.0 mm
Aluminium	1.70 mm	2.5 mm
Lead	0.40 mm	1.5 mm
Wood	5.60 mm	6.5 mm

The Electronics Division, BARC, has a standard point cobalt-60 source which was presently used for the calibration of the TLD's. This consists of a cylindrical (6 mm diameter, 6 mm height) capsule sealed in aluminium, the overall dimensions being 8 mm diameter and 9 mm height (28). The source is supported 4 ft. above ground level and located at the centre of a hall of dimensions 30 ft x 30 ft x 30 ft to minimise scattering. The TLD calibration samples were placed 30 cm. away from the source at the same level and irradiated for a known time. The total exposure received by each sample was obtained in roentgens from the known source strength. The energy absorbed per unit mass by the TLD samples was then calculated in rads from

$$E_D = 0.88 * X^c * \frac{(\frac{\mu_{en}}{\rho})_m}{(\frac{\mu_{en}}{\rho})_{air}} * f * e^{-\mu x} \text{ rads} \qquad (4.1)$$

where 0.88 is the conversion factor for roentgens to rads.

X^c is gamma exposure in roentgens after correction for source decay.

$(\frac{\mu_{en}}{\rho})_m$ is the mass energy absorption coefficient of capsule material at 1.25 Mev.

$(\frac{\mu_{en}}{\rho})_{air}$ is the mass energy absorption coefficient of air at 1.25 Mev.

f is the factor calculated by Equation (2.11)

and $e^{-\mu x}$ is a correction for build-up material attenuation, x being the provided build-up thickness and μ the linear attenuation coefficient.

4.4 TLD READER

Several high-quality commercial TLD readers are available. Figure 4.3 gives a schematic diagram for the system presently used. For carrying out a reading, the TLD powder was placed on the Kanthal strip which could be heated uniformly in a light-tight enclosure by a constant-current power supply. The TL emission produced was sensed by the photomultiplier tube, the signal being amplified by a D.C. amplifier and recorded on a Digilog recorder. Plate 6 gives a general view of the TLD reader set-up, while Plate 7 is a close-up view of the TLD - reader photomultiplier tube with the TLD powder seen uniformly spread out on the Kanthal strip.

The response of a TLD is obtained from the reader in the form of a glow curve, i.e. TL intensity-vs-temperature/time. For taking the reading, either the area under the glow curve or the maximum peak height may be taken as proportional to the dose. The latter parameter was presently used. Figure 4.4 shows typical glow curves obtained for CaF_2 and LiF in the course of the present experiments.

4.5 TEMPERATURE MEASUREMENT SET-UP

The temperature measurement set-up used in conjunction with each thermocouple assembly (Sec. 4.2) consisted of a potentiometer voltmeter bridge (PVB), a selector switch, and an ice bath (Plate 8). The PVB (e.s.i. Model 300) measured the potential difference developed across each thermocouple (40 microvolt/^{o}C) to an accuracy of $\pm$ 1 microvolt. The selector switch selected the particular thermocouple being read. Ice used for the ice bath was prepared from distilled water and the cold thermocouple ends dipped in mercury contained in separate test tubes inserted in the ice. Figure 4.5 shows the thermocouple connections for measurement of (a) absolute temperatures and (b) temperature differences.

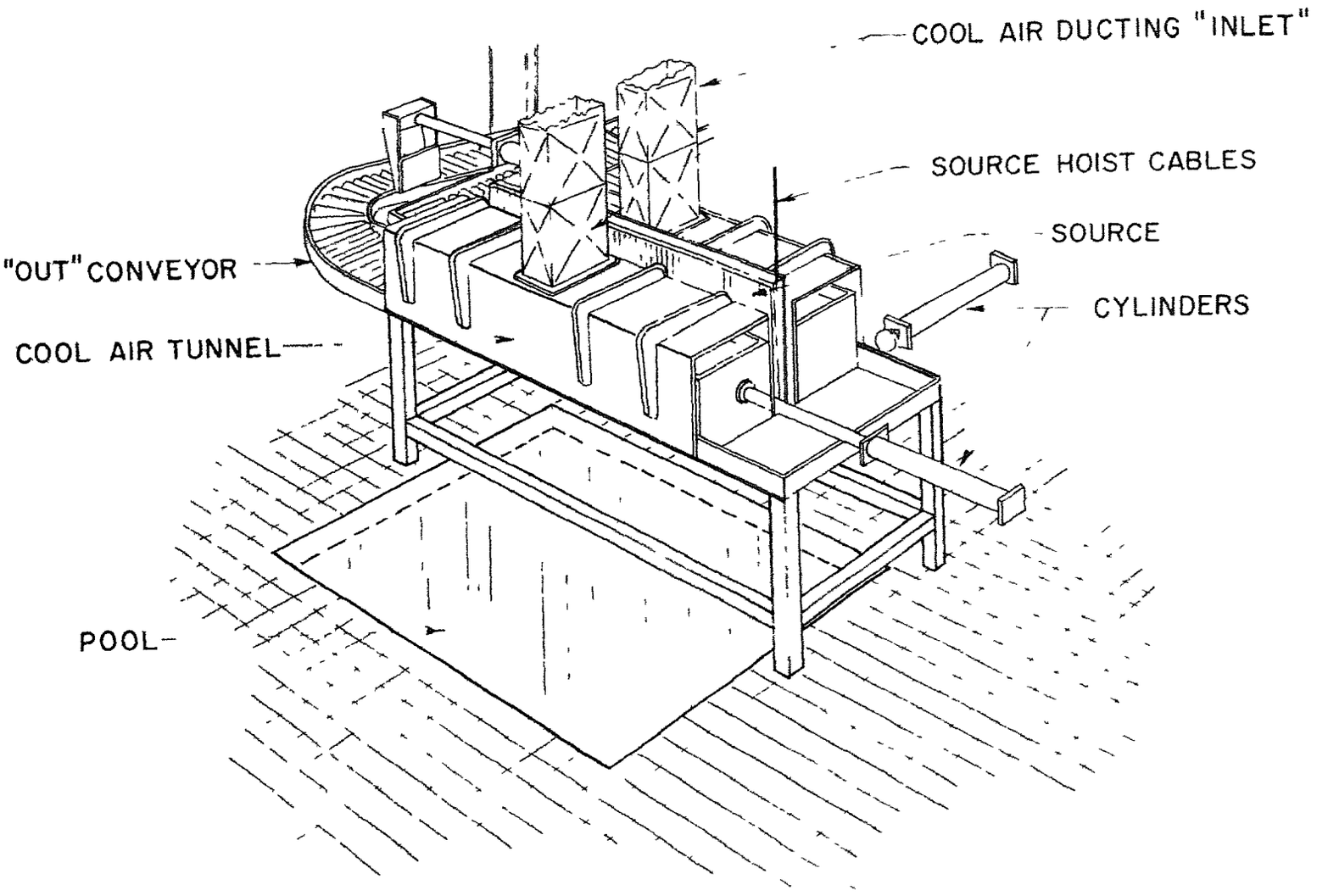

FIG 4.1 THE FIPLY FACILITY

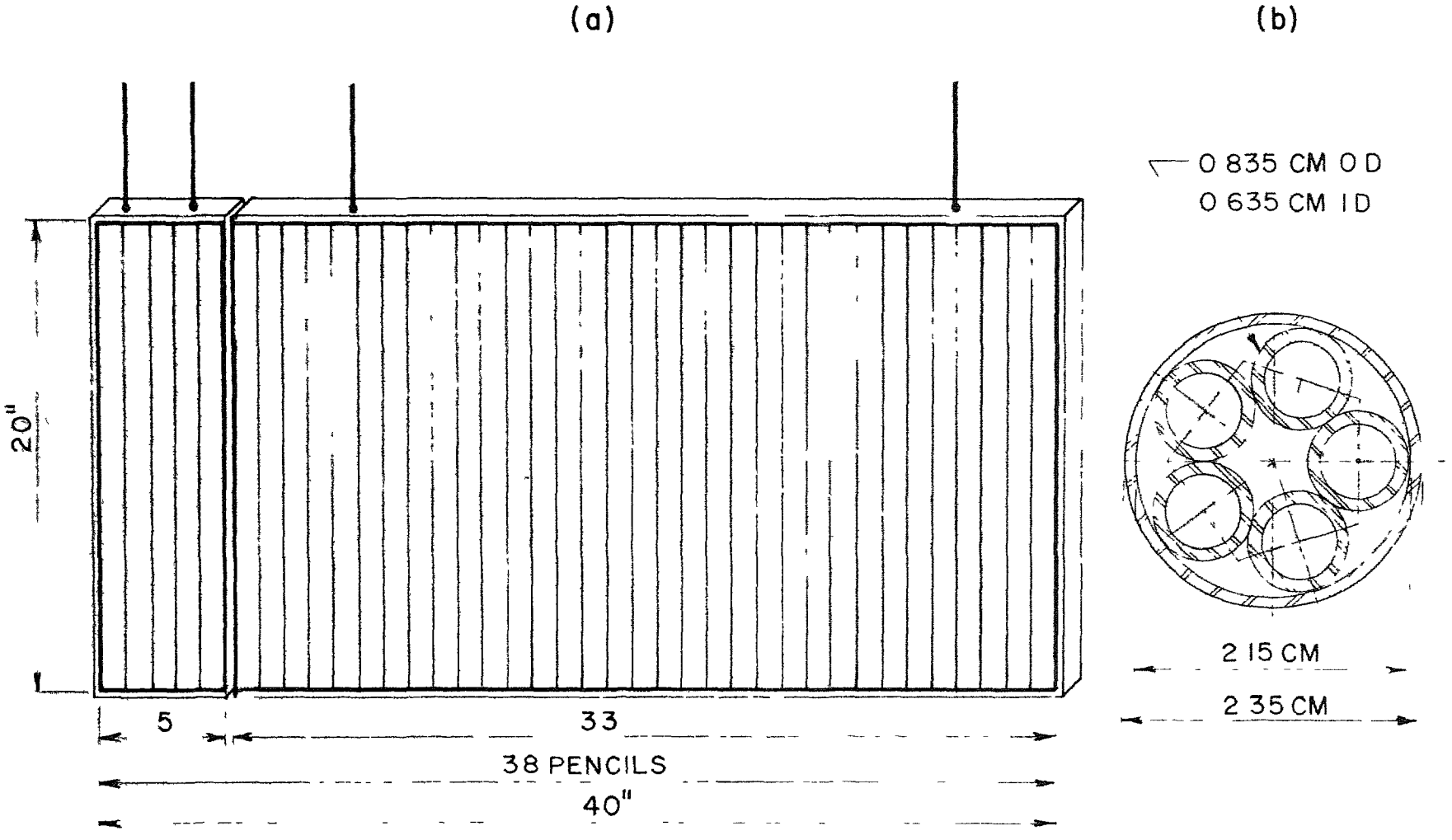

FIG 4 2 ARRANGEMENT OF CO-60 PENCILS IN THE FIPLY SOURCE

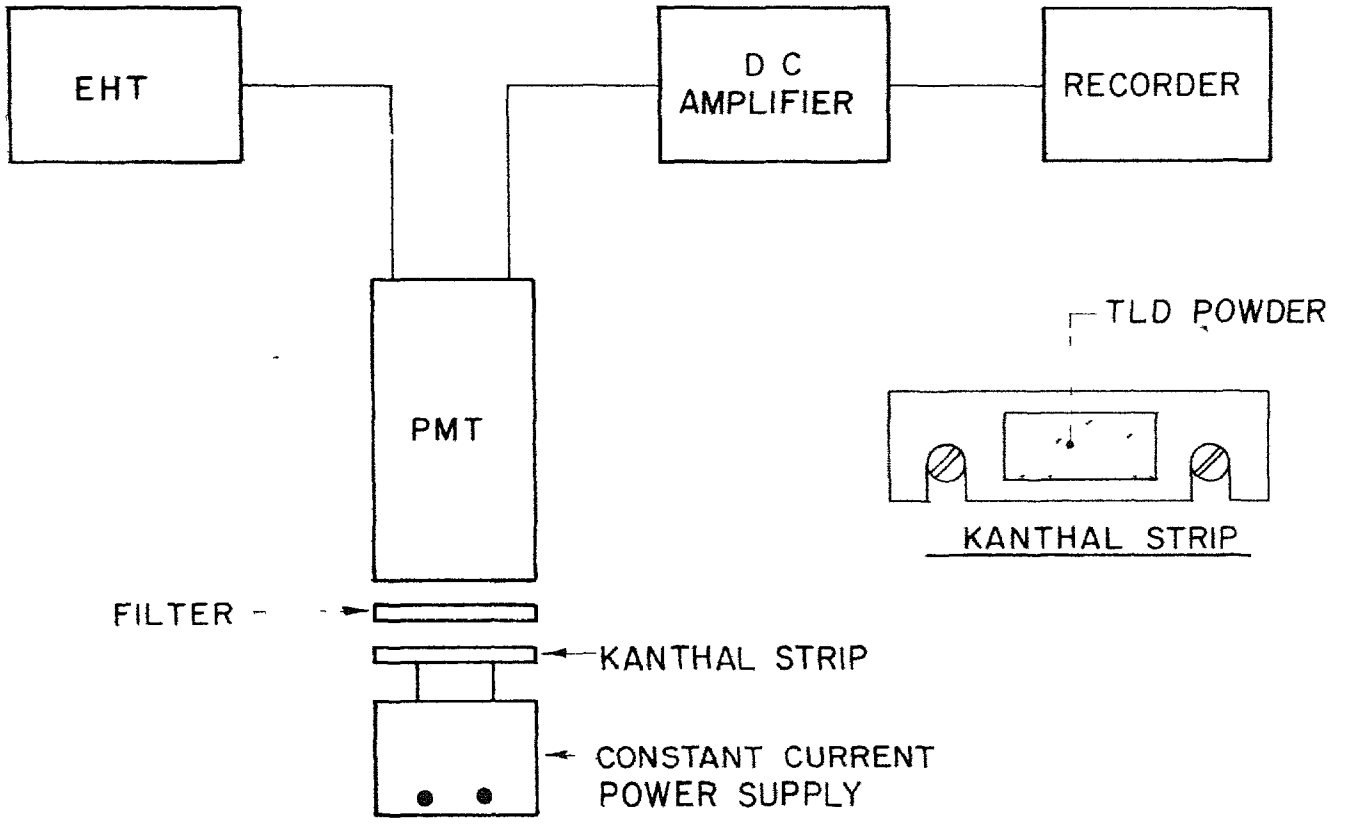

FIG 43 SCHEMATIC DIAGRAM OF TLD READER

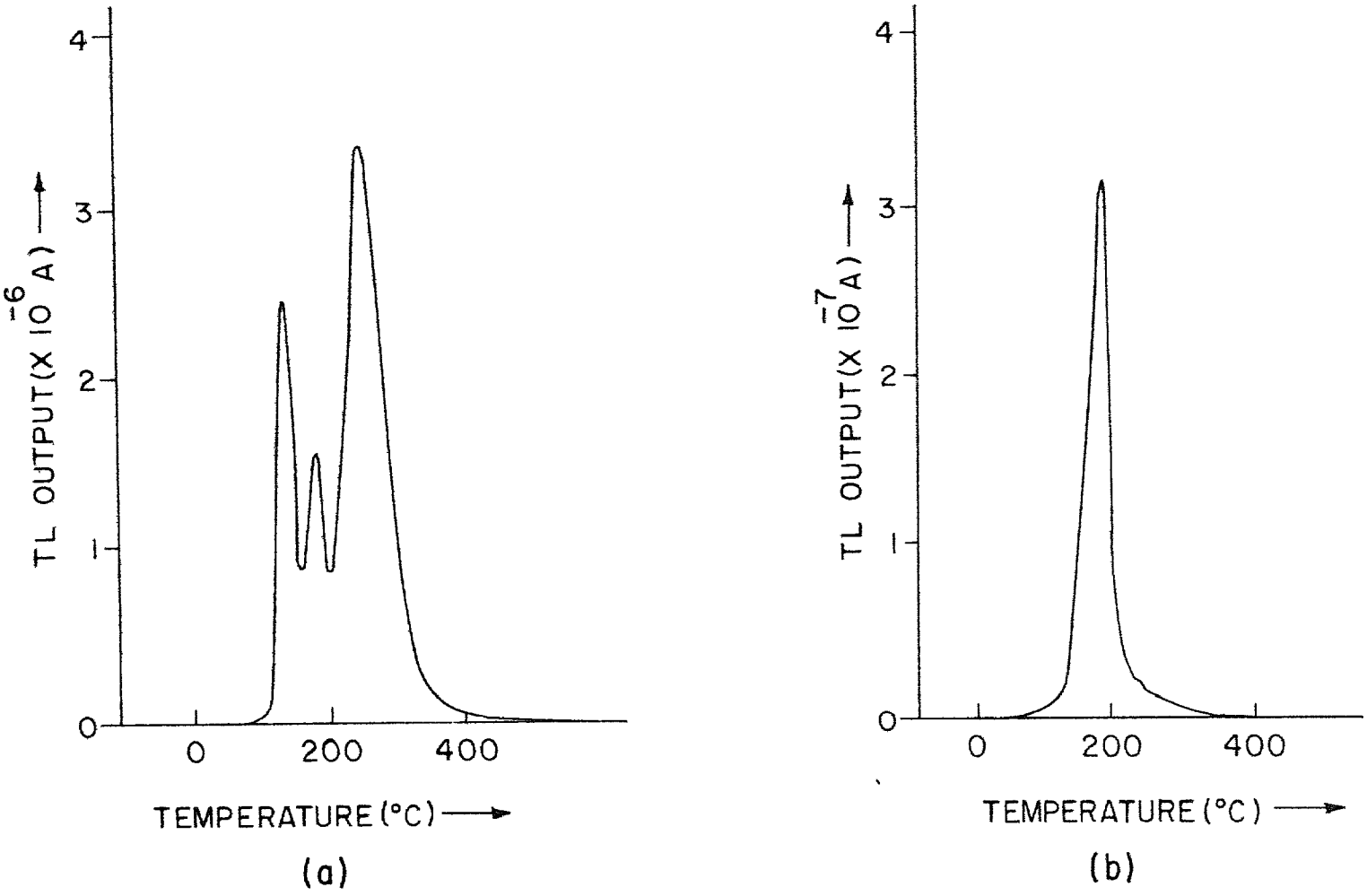

FIG 4 4 TYPICAL GLOW CURVE FOR (a) CaF_2, (b) LiF

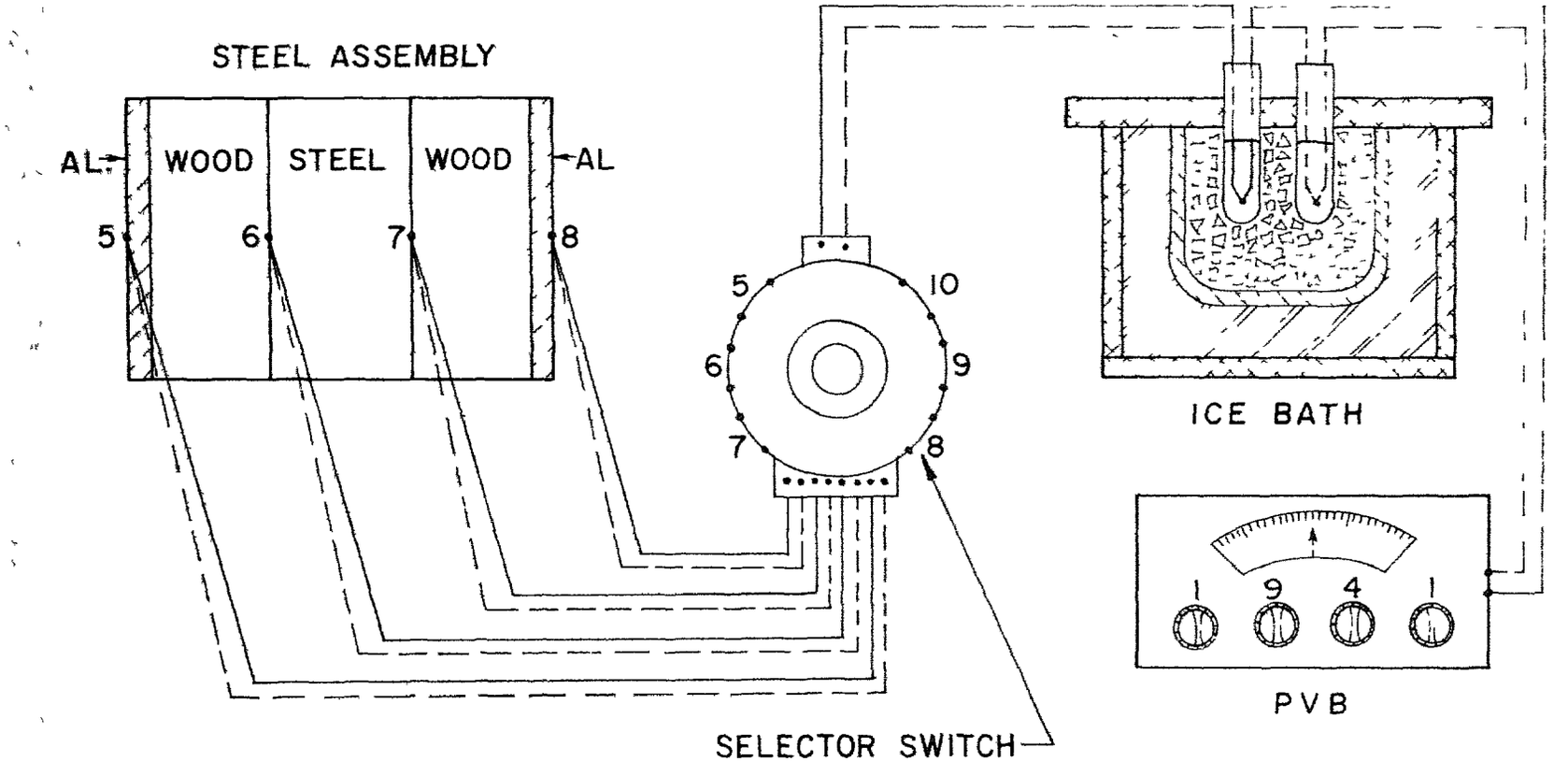

FIG 4·5 (a) THERMOCOUPLES CONNECTIONS FOR MEASUREMENT OF ABSOLUTE TEMPERATURE

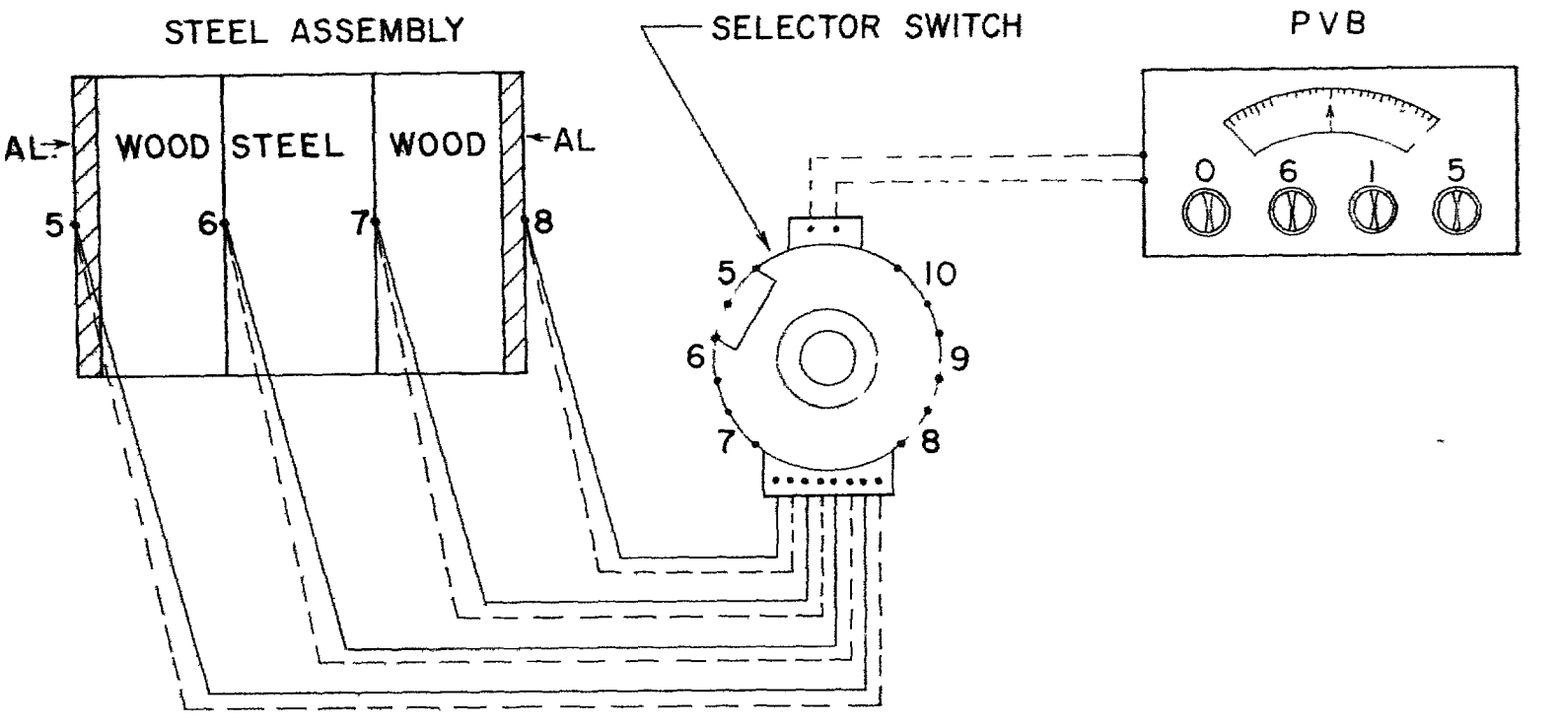

FIG 4 5 (b) THERMOCOUPLES CONNECTIONS FOR MEASUREMENT OF TEMPERATURE DIFFERENCE

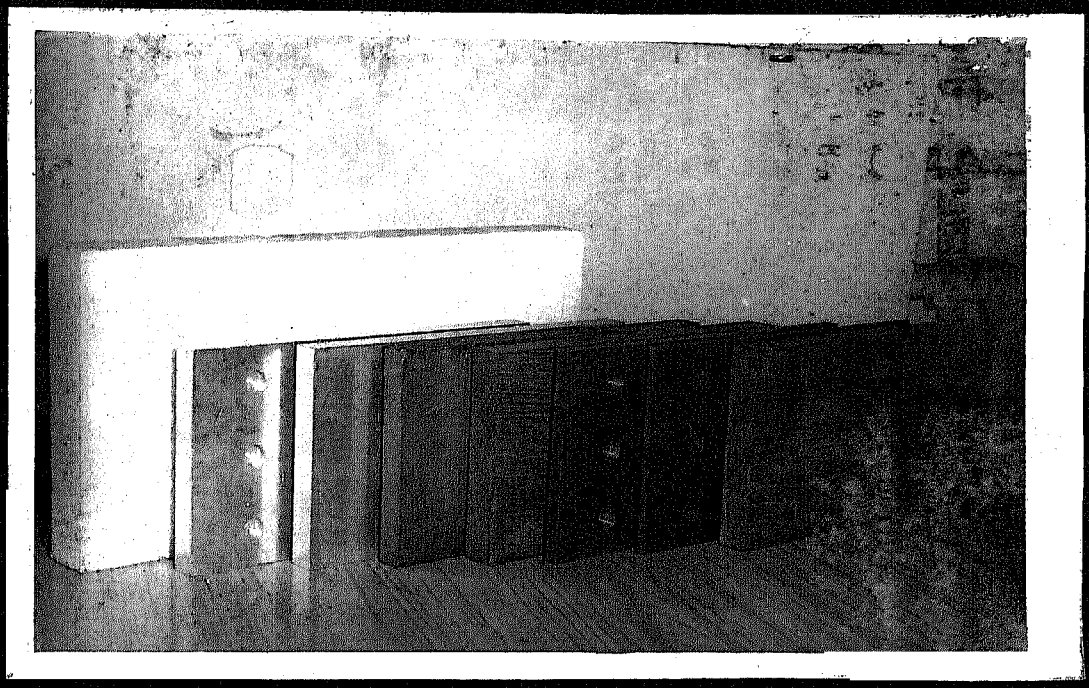

PLATE 3 : Various Experimental Plates

PLATE 4 : Various Blanks for TLD's

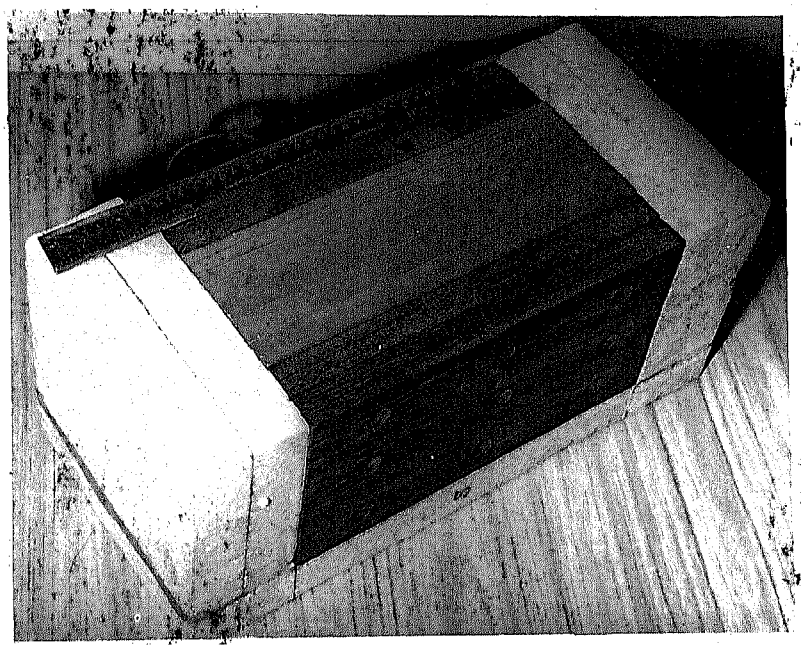

PLATE 5 : The Partly Assembled Aluminium TLD Assembly

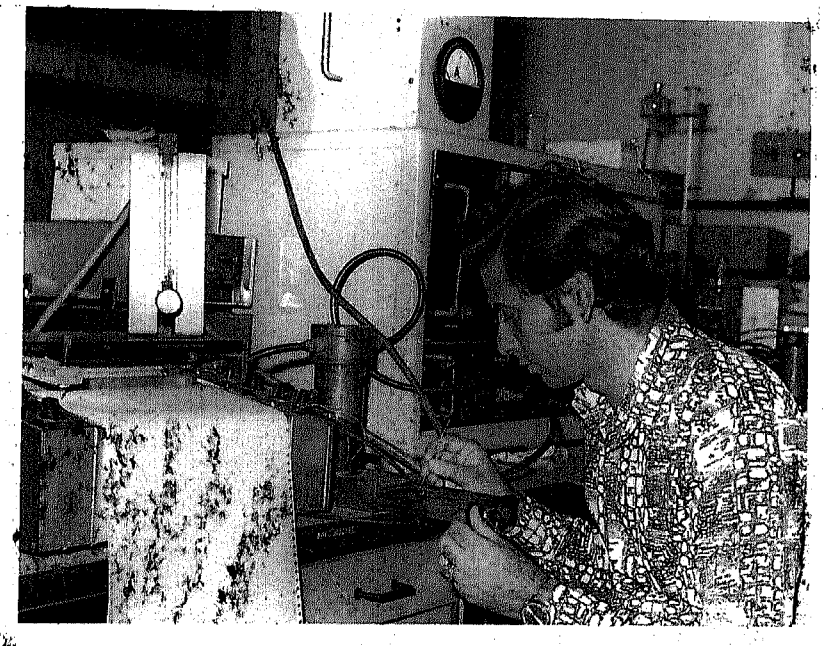

PLATE 6 : General View of the TLD Reader Set-up

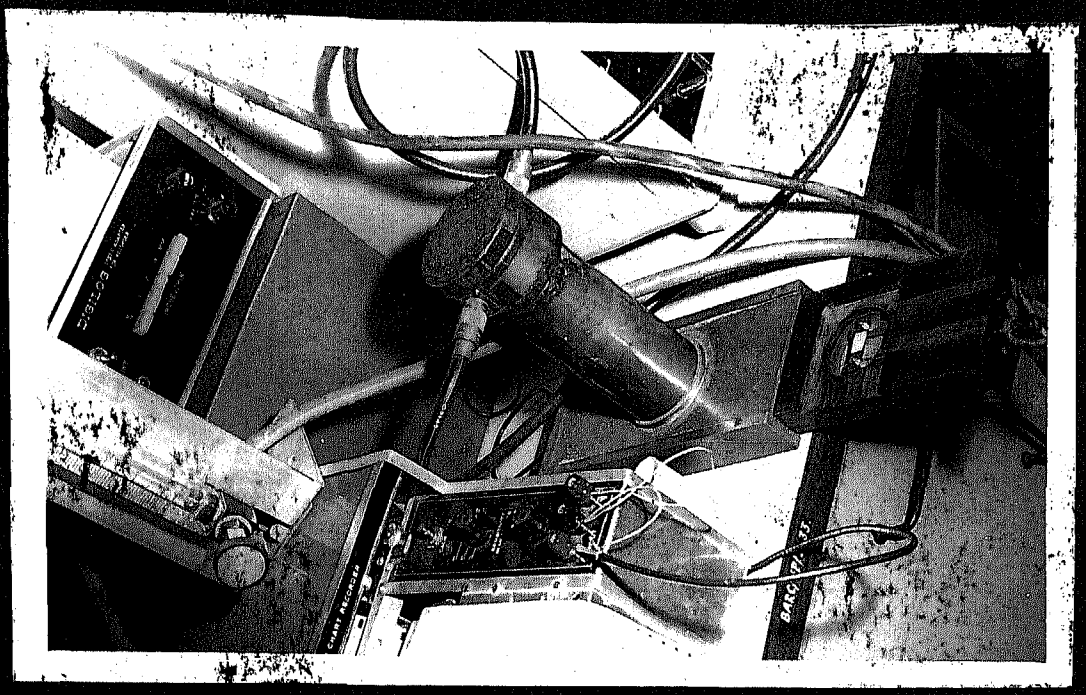

PLATE 7 : Close-up View of the TLD Reader Photomultiplier Tube

PLATE 8 : The Temperature Measurement Set-up

CHAPTER 5

RESULTS AND THEIR DISCUSSION

5.1 TLD'S USED

Natural CaF_2 and LiF TLD's in the form of powder were used for the present work. These were prepared indigenously by the Health Physics Division, B.A.R.C., the size of the grains for these powders being between 80 - 200 mesh. The effective densities of the CaF_2 and LiF powders were determined as 2.66 gm/cm^3 and 1.95 gm/cm^3, respectively. Standard annealing procedures were adopted before using the TLD's for dose measurements. Essentially the pre-irradiation annealing involved heating of the TLD powder in an oven at 400 ^oC for one hour, followed by storage at 80 ^oC for 24 hours. Fading tendencies of the TLD's were rendered negligible by the annealing.

5.2 CALCULATION OF f_s, f_l and f

The deduction of energy absorbed by a material from dose measurements made using TLD's is dependent on the calculation of an appropriate $\frac{1}{f}$ - factor for use in Equation (2.1) (Section 2.3). Equation (2.11) expresses f in terms of the small-cavity and large-cavity values f_s and f_l, respectively, for a given situation.

To calculate $f_s(T_\gamma)$, the electron-flux-dependent small-cavity values have to be averaged over the three primary-electron-spectrum components produced by the monoenergetic gamma-ray of energy T_γ (In the present case of ^{60}Co gammas, only photoelectric and Compton-interactions need be considered). Electron mass stopping powers to enable the deduction of $f_s(T_\gamma)$ from Equations (2.3) and (2.4) have been tabulated by Berger and Seltzer (29, 30). These references were presently used to provide the appropriate (18) mass stopping powers for steel, aluminium, lead and LiF. For CaF_2, for which data was not directly available, stopping powers for aluminium and argon were suitably averaged since the effective atomic number (16.3) for CaF_2 falls between these two elements. The stopping power for wood was obtained assuming an average weight composition of 50% C, 44% O and 6% H (31).

For the evaluation of $f_1(T_\gamma)$ from Equation (2.6), tabulated values of mass energy absorption coefficients for steel, aluminium and lead were taken from Reference (23). Values for wood were obtained by assuming the earlier-stated C/O/H composition. Reference (32) gave mass energy absorption coefficients for CaF_2 and LiF.

Values of f_s and f_l for CaF_2/steel, CaF_2/Al, CaF_2/lead, CaF_2/wood, LiF/steel, LiF/Al, LiF/lead and LiF/wood were calculated for twelve different gamma-energy values. These corresponded to the mean energies for the twelve photon-energy groups presently considered, in the range 0.05-1.40 Mev, for calculating the energy spectrum of the ^{60}Co gamma-rays at different locations. Table 5.1 gives the gamma-energy group structure used, while Table 5.2 exemplifies the calculation of f_s, f_l values for the case of CaF_2/steel.

TABLE 5.1 Gamma-Energy Group Structure

Energy Group	Energy Range (Mev)	Mean Energy (Mev)
1	1.4 - 1.1	1.25
2	1.1 - 0.9	1.00
3	0.9 - 0.7	0.80
4	0.7 - 0.5	0.60
5	0.5 - 0.3	0.40
6	0.3 - 0.2	0.25
7	0.2 - 0.15	0.175
8	0.15- 0.10	0.125
9	0.10- 0.08	0.090
10	0.08- 0.07	0.075
11	0.07- 0.06	0.065
12	0.06- 0.05	0.055

TABLE 5.2 Variation of f_s and f_1 with energy for CaF_2/steel

Energy Group	Mean γ-energy T_1 (Mev)	$(\frac{\mu_{en}}{\rho})_{CaF_2}$	$(\frac{\mu_{en}}{\rho})_{Fe}$	f_1	T_{C1} (Mev)	(S.P.) CaF_2 at T_1	(S.P.) Fe at T_i	^pf_s	^cf_s	f_s
1	1.25	0.0266	0.0249	1.068	0.59	1.414	1.334	1.060	1.057	1.057
2	1.00	0.0278	0.0262	1.061	0.44	1.417	1.337	1.059	1.057	1.058
3	0.80	0.0289	0.0273	1.059	0.32	1.435	1.356	1.058	1.057	1.057
4	0.60	0.0295	0.0286	1.031	0.22	1.484	1.403	1.057	1.061	1.061
5	0.40	0.0301	0.0308	0.977	0.12	1.614	1.526	1.057	1.067	1.067
6	0.25	0.0311	0.0415	0.749	0.06	1.890	1.783	1.060	1.073	1.073
7	0.175	0.0355	0.0654	0.543	0.0352	2.241	2.109	1.062	1.083	1.077
8	0.125	0.0565	0.1502	0.376	0.0205	2.715	2.548	1.066	1.090	1.076
9	0.090	0.0995	0.3165	0.314	0.0116	3.235	3.027	1.069	1.107	1.081
10	0.075	0.1652	0.5507	0.300	0.0084	3.637	3.397	1.071	1.125	1.082
11	0.065	0.2457	0.8242	0.298	0.0065	4.001	3.730	1.073	1.132	1.079
12	0.055	0.3890	1.3005	0.299	0.0048	4.485	4.174	1.074	1.149	1.079

Note: (i) (S.P.) denotes mass stopping power for electrons of energy T_1

(ii) ^cf_s was obtained as the ratio of mass stopping powers for electrons of energy T_{Ci}, the effective Compton-electron energy for the ith group (18).

The weighting factor d in Eqn. (2.11) was calculated by Eqn. (2.9), the effective mass absorption coefficient β being given by Equation (2.7). The value of g used in Eqn. (2.9) was calculated for the LiF, CaF_2 TLD's as exemplified by the following procedure for CaF_2:

Average weight of CaF_2 powder obtained from dispenser, $w = 0.054$ gm

Effective density of CaF_2 powder, $\rho = 2.66$ gm/cm^3

Volume of CaF_2 in blank, $V = \frac{w}{\rho} = 0.0203$ cm^3

Diameter of hole in blank, $d = 0.3$ mm (0.2 mm for lead blanks)

Height of CaF_2 powder in blank, $h = \frac{V}{\frac{\pi}{4} d^2} = 0.287$ cm (0.646 cm for lead blanks)

Average path length of electrons, $g = \frac{4V}{S} = \frac{4 (\frac{\pi}{4} d^2 h)}{(\frac{\pi}{2} d^2 + \pi d h)}$

$= 0.197$ cm (0.173 for lead blanks)

$= 0.525$ gm/cm^2 (0.460 gm/cm^2 for lead blanks)

The g value for LiF powder was similarly obtained as 0.405 gm/cm^2 (0.281 gm/cm^2 for lead blanks).

With the values of β , g known, d was calculated for each of the twelve gamma-energy values and

$f(T_\gamma)$ evaluated from Eqn. (2.11) for all the various combinations. The results are typified by Table 5.3 which gives the values of $\frac{1}{f(T_\gamma)}$ for CaF_2/steel. Curves giving the variation of $\frac{1}{f(T_\gamma)}$ with gamma-energy for the CaF_2 TLD surrounded by steel, aluminium, lead and wood are shown in Fig. 5.1, while Fig. 5.2 gives similar curves for the LiF TLD.

TABLE 5.3 Calculation of $\frac{1}{f(T_\gamma)}$ for CaF_2/steel Combination

Energy Group	$\mathcal{E}$	d	f_s	(1 - d)	f_1	$f(T_\gamma)$	$1/f(T_\gamma)$
1	12.2	0.156	1.057	0.844	1.068	1.067	0.937
2	16.8	0.113	1.058	0.887	1.061	1.061	0.943
3	23.3	0.082	1.057	0.918	1.059	1.059	0.945
4	35.7	0.053	1.061	0.947	1.031	1.033	0.968
5	66.1	0.029	1.067	0.971	0.977	0.980	1.021
6	138	0.014	1.073	0.986	0.749	0.754	1.327
7	242	0.008	1.077	0.992	0.543	0.547	1.829
8	471	0.004	1.076	0.996	0.376	0.379	2.640
9	1000	0.002	1.081	0.998	0.314	0.316	3.167
10	1480	0.001	1.082	0.999	0.300	0.301	3.324
11	2290	0.001	1.079	0.999	0.298	0.299	3.348
12	4100	0.000	1.079	1.000	0.299	0.299	3.340

Note: The values of f are seen to be relatively insensitive to f_s.

5.3 CALCULATION OF GAMMA-SPECTRA

The various experimental assemblies (Section 4.2) consisted of a number of individual plates of different materials. Gamma spectra at the centre of each plate were calculated using the ANISN code (Section 3.2), S_4, P_o approximations being presently employed.

For modelling purposes, the FIPLY source (Fig. 4.2) was taken as a distributed source of gamma-rays belonging to the first energy group, viz. 1.1 - 1.4 Mev. (corresponding to the mean energy of 1.25 Mev for ^{60}Co gamma's). The homogenisation of the source region for obtaining appropriate photon cross-sections was carried out as follows:

Area of 5 cobalt slugs of 0.635 cm. dia = 1.58 cm^2

Area of S.S. cladding = 2.02 cm^2

Total area = 3.60 cm^2

Area of 2.35 cm square = 5.52 cm^2

Effective density of homogenised source region = $\frac{3.60}{5.52} \times 8.0 = 5.2$ gm/cm^3

Photon cross-sections (absorption and total) for the source region (with the above effective density), as well as for steel, aluminium, lead and wood (of measured densities) were obtained from Reference (23). Group scattering cross-sections for the different materials were calculated using Eqn. (3.2) (Section 3.2).

Cross-sections for wood were calculated assuming the earlier mentioned weight composition of 50% C, 44% O and 6% H. Table 5.4 exemplifies the results for the group-to-group scattering cross-sections, the calculated values for steel being shown there.

ANISN-calculated gamma-spectra at characteristic depths for the five different experimental assemblies (Sec. 4.2) are shown plotted in Figs. 5.3 - 5.7.

A separate ANISN calculation was carried out to estimate the spectrum of gamma-rays emerging from the source region in the absence of any assembly. This is shown plotted in Fig. 5.7(a). The fraction of unscattered (Group 1) gamma-rays in this spectrum was $\sim 60\%$. This is of the same order of magnitude as the results reported by Visser and Mouton (33), on the basis of experimental spectrum measurements of gamma-rays from a large ^{60}Co source. Certain numerical checks were also carried out for the ANISN calculations, e.g., use of an S_8-approximation (instead of S_4) was found to have insignificant effect on the computed spectra.

With the gamma-spectrum estimated at the centre of the various plates of each assembly, flux-weighted $\frac{1}{f}$ - values for each location were calculated using Eqn. (2.12). Tables 5.5 - 5.9 give the $\frac{1}{f}$ - values calculated for various depths in the five different assemblies.

TABLE 5.4 Gamma Scattering (Group-to-Group) Cross-Sections for Iron

L.G. No.	Group 1	Group 2	Group 3	Group 4	Group 5	Group 6	Group 7	Group 8	Group 9	Group 10	Group 11	Group 12
1.	.0526	-	-	-	-	-	-	-	-	-	-	-
2.	.0667	.0547	-	-	-	-	-	-	-	-	-	-
3.	.0648	.1020	.0844	-	-	-	-	-	-	-	-	-
4.	.0679	.0962	.1499	.1450	-	-	-	-	-	-	-	-
5.	.0921	.1143	.1485	.2396	.2970	-	-	-	-	-	-	-
6.	.0718	.0981	.1231	.1526	.2437	.3631	-	-	-	-	-	-
7.	-	-	.0116	.0523	.1575	.2756	.3808	-	-	-	-	-
8.	-	-	-	-	-	.1929	.5489	.6272	-	-	-	-
9.	-	-	-	-=	-	-	-	.4120	.4835	-	-	-
10.	-	-	-	-	-	-	-	-	.4634	.4483	-	-
11.	-	-	-	-	-	-	-	-	.1645	.3803	.6020	-
12.	-	-	-	-	-	-	-	-	-	.3251	.5858	1.2180

Note: L.G. denotes the lower-energy group for the scattering.

TABLE 5.5 Flux-weighted values of $\frac{1}{f}$ in Steel Assembly for CaF_2 and LiF TLD'S

Assembly Depth (cm)	Material	CaF_2	LiF
1.70	Wood	0.950	1.061
4.20	Wood	0.944	1.060
5.35	Steel	1.219	1.584
5.95	Steel	1.214	1.524
6.55	Steel	1.212	1.506
7.15	Steel	1.222	1.520
7.75	Steel	1.226	1.532
8.45	Steel	1.225	1.527
9.45	Steel	1.236	1.572
11.7	Wood	0.930	1.057
14.2	Wood	0.926	1.051

TABLE 5.6 Flux-weighted Values of $\frac{1}{f}$ in Aluminium Assembly for CaF_2 and LiF TLD'S

Assembly Depth (cm)	Material	CaF_2	LiF
1.70	Wood	0.892	1.047
4.20	Wood	0.864	1.042
5.60	Al	0.841	1.179
6.60	Al	0.828	1.201
7.60	Al	0.816	1.219
8.60	Al	0.806	1.238
10.60	Al	0.795	1.260
12.60	Al	0.743	1.281
14.60	Al	0.777	1.306
16.70	Wood	0.724	1.011
19.20	Wood	0.732	1.012

TABLE 5.7 Flux-weighted Values of $\frac{1}{f}$ in Lead Assembly for CaF_2 and LiF TLD'S

Assembly Depth (cm)	Material	CaF_2	LiF
1.70	Wood	0.987	1.067
4.20	Wood	0.992	1.067
5.35	Lead	1.866	1.683
5.95	Lead	1.616	1.432
6.55	Lead	1.553	1.368
7.15	Lead	1.501	1.326
7.75	Lead	1.555	1.375
9.70	Wood	1.054	1.079
12.20	Wood	1.050	1.078

TABLE 5.8 Flux-weighted Values of $\frac{1}{f}$ in Combination-1 for CaF_2

Assembly Depth (cm)	Material	CaF_2
1.70	Wood	0.952
4.20	Wood	0.948
5.45	Steel	1.211
6.45	Steel	1.261
8.70	Wood	0.880
11.20	Wood	0.855
12.60	Al	0.836
13.60	Al	0.826
14.60	Al	0.820
15.60	Al	0.815
17.70	Wood	0.774
20.20	Wood	0.784

TABLE 5.9 Flux-weighted Values of $\frac{1}{f}$ in Combination-2 for CaF_2

Assembly Depth (cm)	Material	CaF_2
1.70	Wood	0.894
4.20	Wood	0.868
5.60	Al	0.844
6.60	Al	0.833
7.60	Al	0.822
8.60	Al	0.814
10.70	Wood	0.794
13.20	Wood	0.813
14.45	Steel	1.332
15.45	Steel	1.294
17.70	Wood	0.884
20.20	Wood	0.884

It is interesting to note that even in the case of a poorly matched combination, such as LiF/lead (Fig. 5.2), the effective $\frac{1}{f}$ - values are not too far from unity. This is due to the filtering out of the low-energy gammas at greater depths within the high-Z material. This results in a harder spectrum for lead than for steel or aluminium (Figs. 5.3 - 5.5) and consequently in not too high a sensitivity on low-energy gammas for which $\frac{1}{f}$ - variations are large.

5.4 DOSE MEASUREMENT EXPERIMENTS

Calibration of the TLD's was carried out before every assembly irradiation by filling four blanks each of steel, aluminium, lead and wood (as appropriate) with CaF_2, and the same number of blanks with LiF. Half the blanks were placed at 30 cm, and the rest at 15 cm, from the standard ^{60}Co calibration source discussed in Section 4.3. Irradiation of these blanks was carried out for a known period of time ($\sim$4 days) to give doses in the same range as that acquired by TLD's during the assembly irradiations (10^3 - 10^4 rads). The doses absorbed by the calibration TLD's were calculated by Eqn. (4.1), and their response obtained from the TLD reader under the same conditions as employed for the assembly TLD's. Typical dose/response curves obtained in the calibration process

are shown in Fig. 5.8, corrections for LiF supralinearity effects being thus explicitly obtained in the range of interest.

It should be mentioned that for normalising the response of the TLD's irradiated in the different plates of each assembly, the calibration TLD's used were those irradiated in blanks of the corresponding material. This was to minimise the relative error in the $\frac{1}{f}$ - corrections that had to be applied for deducing heat-generation rates in the plates.

The FIPLY irradiation procedure for dose measurements in the various assemblies (Table 4.1) was essentially the same as described below for the case of the steel assembly.

Five wood blanks filled with TLD powder were placed in five different holes (the central and the four corner positions) in the first wood plate. The remaining holes in the plate carried wood blanks without TLD's. Similarly another five blanks with TLD's were located in the second wood plate, at the central and the four middle positions. The first steel plate carried five steel blanks containing TLD powder in the same positions as for the first wood plate, the second steel plate having five in the second set of positions. In this way, each

of the plates forming the assembly carried five TLD-containing blanks of the appropriate material, the set of positions alternating between the two mentioned above.

The assembly was irradiated for 1 minute of steady exposure (with the source in the fully-up position). After the irradiation, the TLD-containing blanks were taken out, and replaced by a second set of blanks containing fresh powder. A second irradiation of the assembly for 2 minutes of steady exposure was then carried out.

The TLD response at each location corresponding to 1 minute of steady exposure had to be corrected for source-transient effects (Section 3.1), and this was achieved by interpreting the various TLD readings as follows:

If S denotes the corrected steady-exposure response (min^{-1}) at a particular location, x the response due to source transients, X_1 the reading obtained from the TLD used in the first irradiation and X_2 that from the second,

$$X_1 = S + x \qquad (5.1)$$

$$X_2 = 2S + x \qquad (5.2)$$

Equations (5.1) and (5.2) were used to eliminate x at each position, giving

$$S = (X_2 - X_1) \qquad (5.3)$$

From the appropriate calibration curve, the above response was expressed in rads/min for the TLD. The average result obtained for the five TLD locations in each plate gave the energy absorbed per minute for the TLD material in the plate. In the first few experiments, it was found that the average value was practically the same as that at the central location and, subsequently, only the central locations were employed.

The heat generation in each plate was obtained in watts/cm^3 of plate material by multiplying the above TLD dose by the appropriate $\frac{1}{f}$ - factor (Section 5.2) and a conversion constant K given by

$$K = \frac{\text{Joule}}{\text{Rad}} * \frac{\text{min}}{\text{sec}} * \frac{\text{gm}}{\text{cm}^3} = 10^{-5} * \frac{1}{60} * \rho = \frac{10^{-6}}{6} \rho \qquad (5.4)$$

ρ being the density of the plate material in gm/cm^3.

Table 5.10 gives the heat generation rates measured in the plates of the steel, aluminium and lead assemblies, using both CaF_2 and LiF. The results are shown graphically in Figs. 5.9 - 5.11, smooth curves having been drawn through the experimental points. These curves are shown normalised to unity at the centre of the assemblies in Figs. 5.12 - 5.14, to enable comparison with gamma-heating results calculated by ANISN. The latter were obtained as a "reaction rate" from the ANISN -

calculated gamma-spectra using "cross-sections" for the ith group given by

$$\Sigma_i = \left(\frac{\mu_{en}}{\rho}\right)_i E_i \qquad (5.5)$$

where $\left(\frac{\mu_{en}}{\rho}\right)_i$ is the mass energy absorption coefficient of the material for gammas of energy E_i, the mean energy of the ith group.

TABLE 5.10 Heat-generation Rates (x 10^{-3}) in Watts/cm^3 Measured with CaF_2 and LiF in Steel, Aluminium and Lead Assemblies

Steel Assembly			Alluminium Assembly			Lead Assembly		
Plates	CaF_2	LiF	Plates	CaF_2	LiF	Plates	CaF_2	LiF
W_1	0.54	0.41	W_1	0.40	0.42	W_1	0.28	0.33
W_2	0.50	0.38	W_2	0.38	0.40	W_2	0.26	0.28
S_1	4.2	5.3	A_1	1.8	1.6	L_1	9.5	6.5
S_2	3.9	3.7	A_2	1.5	1.3	L_2	4.3	4.0
S_3	3.1	3.0	A_3	1.1	1.2	L_3	1.9	2.2
S_4	2.6	2.8	A_4	1.2	1.1	L_4	1.4	1.8
S_5	2.1	1.8	A_5	0.9	0.9	L_5	1.3	1.2
S_6	1.6	1.2	A_6	0.6	0.6	W_3	0.05	0.05
S_7	1.2	0.9	A_7	0.5	0.4	W_4	0.05	0.05
W_3	0.09	0.05	W_3	0.12	0.10			
W_4	0.08	0.05	W_4	0.11	0.09			

(Notation for plates: W = wood, S = steel, A = aluminium, L = lead).

It is seen from Table 5.10 that the heat generation rates obtained from CaF_2 and LiF measurements are in reasonable agreement with each other, except for a few locations. While some of the differences may be attributed to random errors in the TLD measurements, significant contribution to the overall error may be expected from the fact that the $\frac{1}{f}$ - factors have been deduced from infinite-slab geometry calculation of the gamma-spectra. This is illustrated, for example, by the heat generation values obtained from CaF_2, LiF in the first lead plate of the lead assembly. With the gamma-spectrum being soft for the lead assembly at this location (Fig. 5.5), the $\frac{1}{f}$ - factor for LiF is subject to greater uncertainty than that for CaF_2 (Figs. 5.1, 5.2). Similar arguments, though to a smaller degree, would justify preference of the CaF_2 results over the LiF - measured values for steel and aluminium also. Accordingly, it was the CaF_2 - measured heat-generation profiles of Figs. 5.9 - 5.11 that were used for providing the input to the HEATING code for the computation of temperature drops.

Heat generation rates in the various plates for Combinations 1 and 2 were measured only with CaF_2 for the above reasons. The results are tabulated in Table 5.11 and shown graphically in Figs. 5.15 and 5.16. Also shown in the figures are the ANISN-calculated heat-generation rates normalised to the experimental values at

the centre of the steel region for Combination-1, and at the centre of the aluminium region for Combination-2. It is seen from these figures, as also from Figs. 5.12-5.14, for the other assemblies, that the ANISN-calculated heat-generation profiles are significantly different from the experimental profiles. This is only to be expected from the infinite-slab nature of the ANISN calculations.

TABLE 5.11 Heat Generation Rates (x 10^{-3}) in Watts/cm^3 Measured with CaF_2 in Combination 1 and 2.

Combination-1		Combination-2	
Plates	Q	Plates	Q
W_1	0.31	W_1	0.43
W_2	0.30	W_2	0.32
S_1	3.9	A_1	1.5
S_2	2.9	A_2	1.4
W_3	0.17	A_3	1.2
W_4	0.15	A_4	1.1
A_1	0.30	W_3	0.20
A_2	0.29	W_4	0.10
A_3	0.32	S_1	2.4
A_4	0.19	S_2	1.8
W_5	0.08	W_5	0.08
W_6	0.07	W_6	0.05

(Notation for plates: W = wood, S = steel, A = aluminium)

5.5 TEMPERATURE DROPS DEDUCED FROM DOSE MEASUREMENTS:

Heat-generation rates in watts/cm^3 obtained from CaF_2 measurements in each assembly were fed as part of the input data to the HEATING code. The density of each material was measured, and corresponding values of thermal conductivity were obtained from standard handbooks (34, 35, 36). Table 5.12 shows the density and thermal-conductivity values used for the various materials.

TABLE 5.12 Density and Thermal Conductivity Values Used for the Various Materials

Material	Density gm/cm^3	Thermal cond. watts/cm °C
Steel	8.0	0.52 (*)
Aluminium	2.8	1.21 (*)
Lead	11.3	0.35 (*)
Wood	0.72	1.63×10^{-3} (**)
Thermocole	0.017	3.37×10^{-4} (***)

* Ref. (34) ** Ref. (35) *** Ref. (36)

Convective heat-transfer boundary conditions, with $h = 11 \times 10^{-3}$ watts/cm^2-°C and $T_{air} = 30$ °C, were used in the HEATING code. The pair of h, T_{air} values was obtained on the basis of consistency with measured

surface temperatures for the steel assembly.* Table 5.13 summarizes the HEATING-calculated, steady-state Δ T-values for the various assemblies, the figure below explaining the notation used for ΔT_1.

(a) Steel, Aluminium, Lead, Assemblies

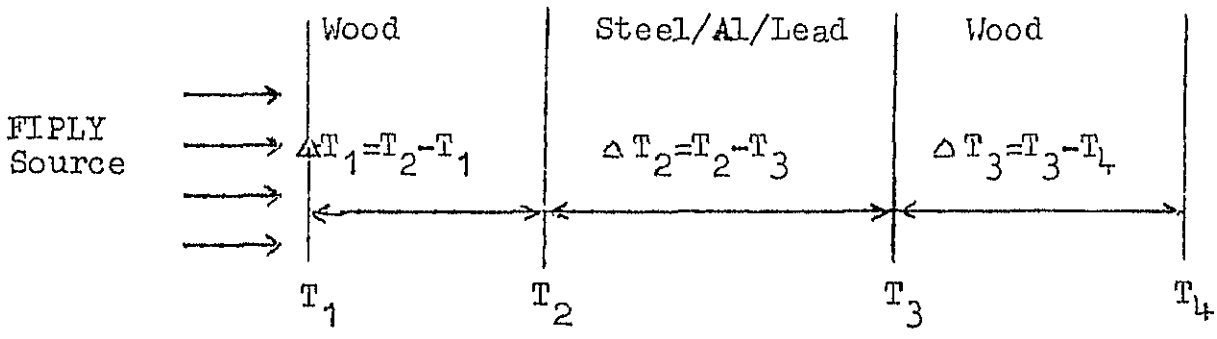

(b) Combinations 1 and 2

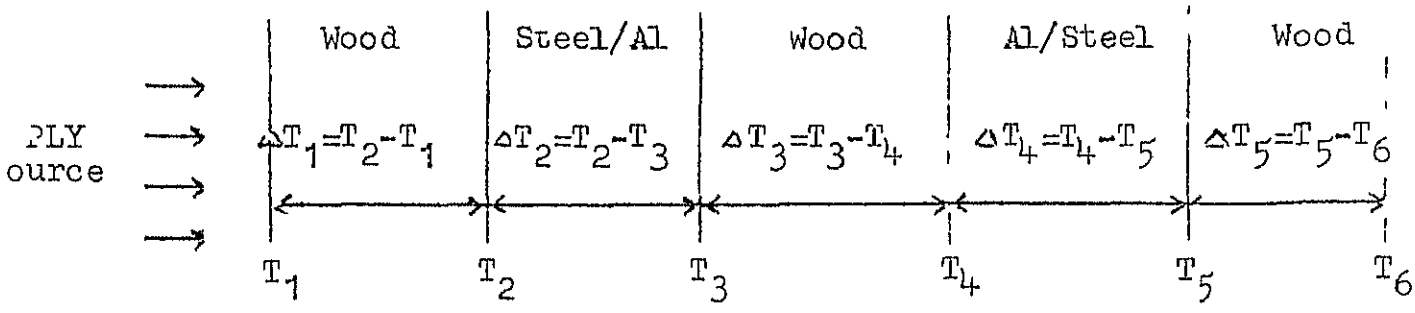

TABLE 5.13 Temperature Drops (^{o}C) Obtained by HEATING Code Through Dose Measurements in Various Assemblies

Assembly	ΔT_1	ΔT_2	ΔT_3	ΔT_4	ΔT_5
Steel	15.3	0.02	15.3	-	-
Aluminium	11.4	0.02	11.4	-	-
Lead	16.2	0 03	16.2	-	-
Combination-1	14.4	0.003	6.6	0.004	8.0
Combination-2	11.8	0.002	1.1	0.01	10.8

*Numerical studies with HEATING showed relatively little sensitivity of the calculated ΔT - values on the assumed values

The HEATING results of Table 5.13 fully justify the design considerations for the present experiments (Sec. 3.1), i.e., the temperature drops across the low-thermal-conductivity material, wood, are of a magnitude that can be easily compared with thermocouple measurements while those across steel, aluminium or lead are not.

5.6 THERMOCOUPLE EXPERIMENTS:

Each thermocouple assembly (Table 4.1) was irradiated in FIPLY continuously for about 30 hours to achieve steady-state conditions. Extreme care was taken in assembling the various plates prior to the irradiation to avoid any possibility of air gaps between them. Another precaution taken was to tape the front and rear surfaces of the assembly to avoid air circulation in any finite gaps between the thermocole insulation and the plates. Thermocouples readings were taken at 30-minute intervals during the irradiation following the procedure discussed in Section 4.5. Both absolute temperatures and ΔT - values were obtained. Fig. 5.17 shows the ΔT_1 transients for the steel, aluminium and lead assemblies, while Figs. 5.18, 5.19 give the ΔT_1, ΔT_3, ΔT_5 transients for Combination 1 and 2, respectively. It is seen that steady-state conditions were achieved in all the experiments.

The ΔT-values in Figs. 5.17-5.19 are seen to not pass through the origin. This was only to be expected

considering that the assembly was typically at $\sim$30 °C, before being introduced into the air-cooled FIPLY irradiation channel with an air-blast temperature of $\sim$25 °C. An experiment was conducted with a thermocouple assembly introduced into the FIPLY channel at time t = 0, the air-cooling being started without the source being brought out. An initial ΔT_1 value of 5 °C was recorded for this experiment and this was found to drop to less than a degree within 8 hours as shown in Table 5.14. Any initial-ΔT effects would thus be quite insignificant after, say 20 hours.

TABLE 5.14 Variation of Initial ΔT_1 with Time

Time in Hrs	ΔT_1 in °C
0	5.0
4	1.9
6	1.4
8	0.9

Table 5.15 summarises the steady-state ΔT_1 - values obtained during the irradiation of the various thermocouple assemblies.

TABLE 5.15 Temperature Drops (°C) Measured by Thermocouples in the Various Assemblies

Assembly	ΔT_1	ΔT_2	ΔT_3	ΔT_4	ΔT_5
Steel	16.0	0.20	16.3	-	-
Aluminium	11.9	0.30	11.9	-	-
Lead	17.0	0.12	17.2	-	-
Combination-1	15.0	0.03	7.1	0.10	8.6
Combination-2	12.5	0.05	2.7	0.03	10.5

5.7 COMPARISION OF DEDUCED AND MEASURED ΔT-VALUES

From Tables 5.13 and 5.15, it is seen that the agreement between dose-deduced and measured temperature drops across the wood is quite satisfactory for all the assemblies, except for the ΔT_3-results for Combination-2. The latter discrepancy is explained by the following fact. While in most of the other cases, HEATING-calculated results are more or less linearly dependent on the gamma-heating measurements for individual regions, the ΔT_3-results for Combination-2 depends on the difference of two nearly equal quantities, viz. the heat generated in the aluminium and steel regions for this assembly (Table 5.11).

Comparison of Tables 5.13 and 5.15 does indicate a systematic trend, viz. that the thermocouple-measured

temperature drops are about 5% greater than those obtained from HEATING. The overall agreement is nevertheless quite satisfactory, considering the various sources of error discussed in the following section.

5.8 DISCUSSION OF ERRORS

Tables 5.16 and 5.17 summarize the sources of systematic and random error in temperature drops deduced from the gamma-heating measurements and those measured directly using thermocouples. The indicated estimates of the individual errors are based on order-of-magnitude considerations for a typical situation, e.g. error in HEATING-deduced ΔT-values have been assumed to be directly related to errors in measured heat-generation rates (not valid for the ΔT_3-results for Combination-2).

TABLE 5.16 Sources of Error in Gamma-heating-deduced ΔT-Values

Source of Error		Error
(a)	Systematic	
	1. Estimation of $\frac{1}{f}$ - factors	± 2%
	2. Calibration of TLD's	± 2%
	3. Thermal-conductivity data for wood and thermocole	± 3%
	4. HEATING code (boundary conditions etc.)	± 2%
(b)	Random (per experiment)	
	1. TLD Dispensing and Reading	± 3%
	2. Effect of Source Transients	± 1%
	3. Positioning of Assembly	± 1%

TABLE 5.17 Sources of Error in Thermocouple-measured ΔT-Values

Source of Error		Error
(a)	Systematic	
	1. Effect of air gaps	+ 2%
	2. Reaching of steady-state	- 1%
	3. Effect of fluctuations in outside temperature	± 1%
	4. Thermocouple-End Heating	+ 1%
	5. Thermocouple Calibration	± 1%
(b)	Random (per experiment)	
	1. Thermocouple Readout	negligible
	2. Positioning of Assembly	± 1%

The overall (r.m.s) errors in the comparison of deduced and measured temperature drops (Section 5.7) have thus been presently estimated to be of the order of ± 5% systematic and ± 3% random.

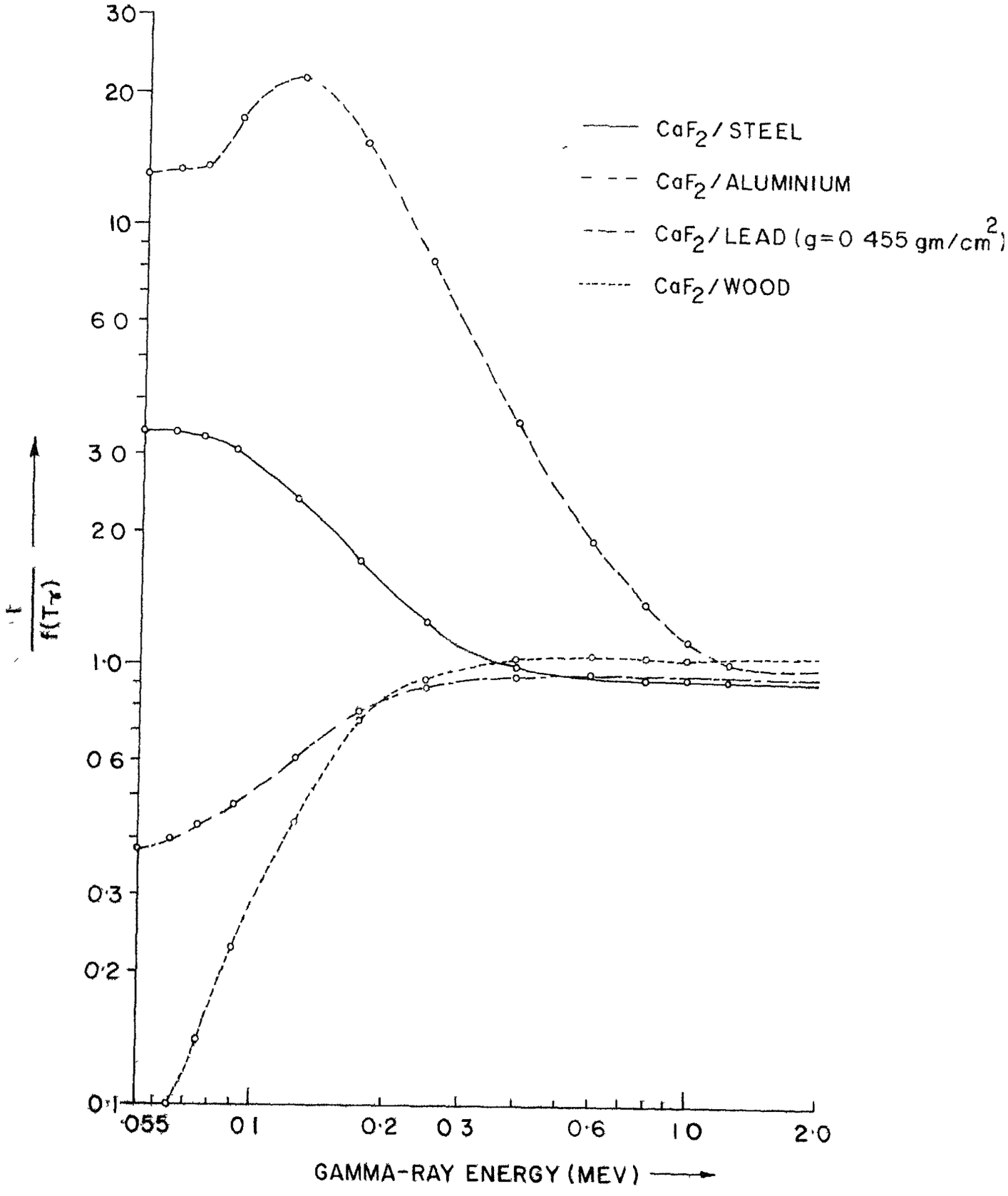

FIG 5.1 VARIATION OF $\frac{1}{f(T_\gamma)}$ AS A FUNCTION OF γ-ENERGY FOR CaF_2 TLD SURROUNDED BY STEEL, ALUMINIUM, LEAD AND WOOD $g = 0.525$ gm/cm^2

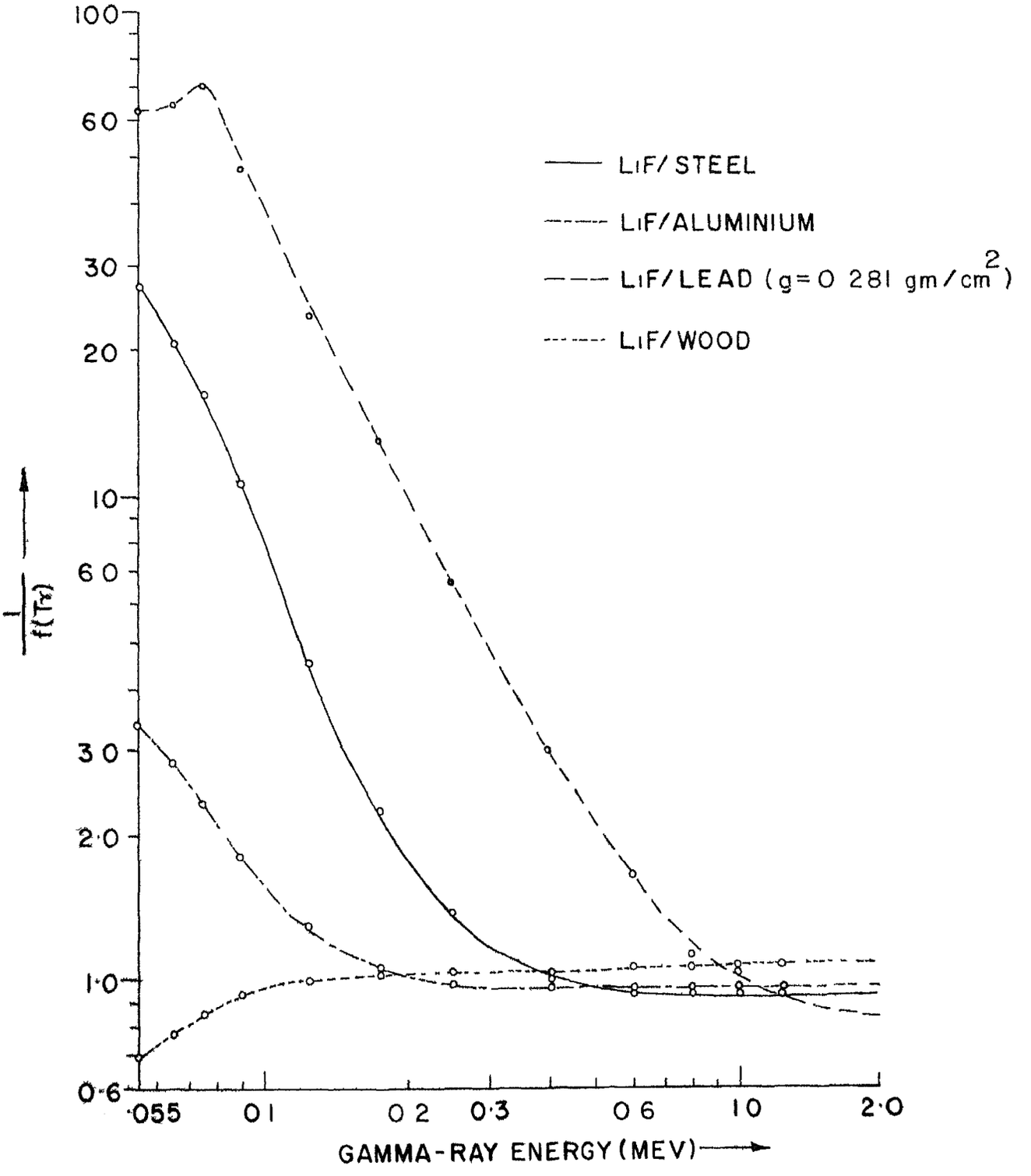

FIG.5·2 VARIATION OF $\frac{1}{f(T\gamma)}$ AS A FUNCTION OF γ-ENERGY FOR LiF TLD SURROUNDED BY STEEL, ALUMINIUM, LEAD AND WOOD

$g = 0{\cdot}405$ gm/cm.^{2}

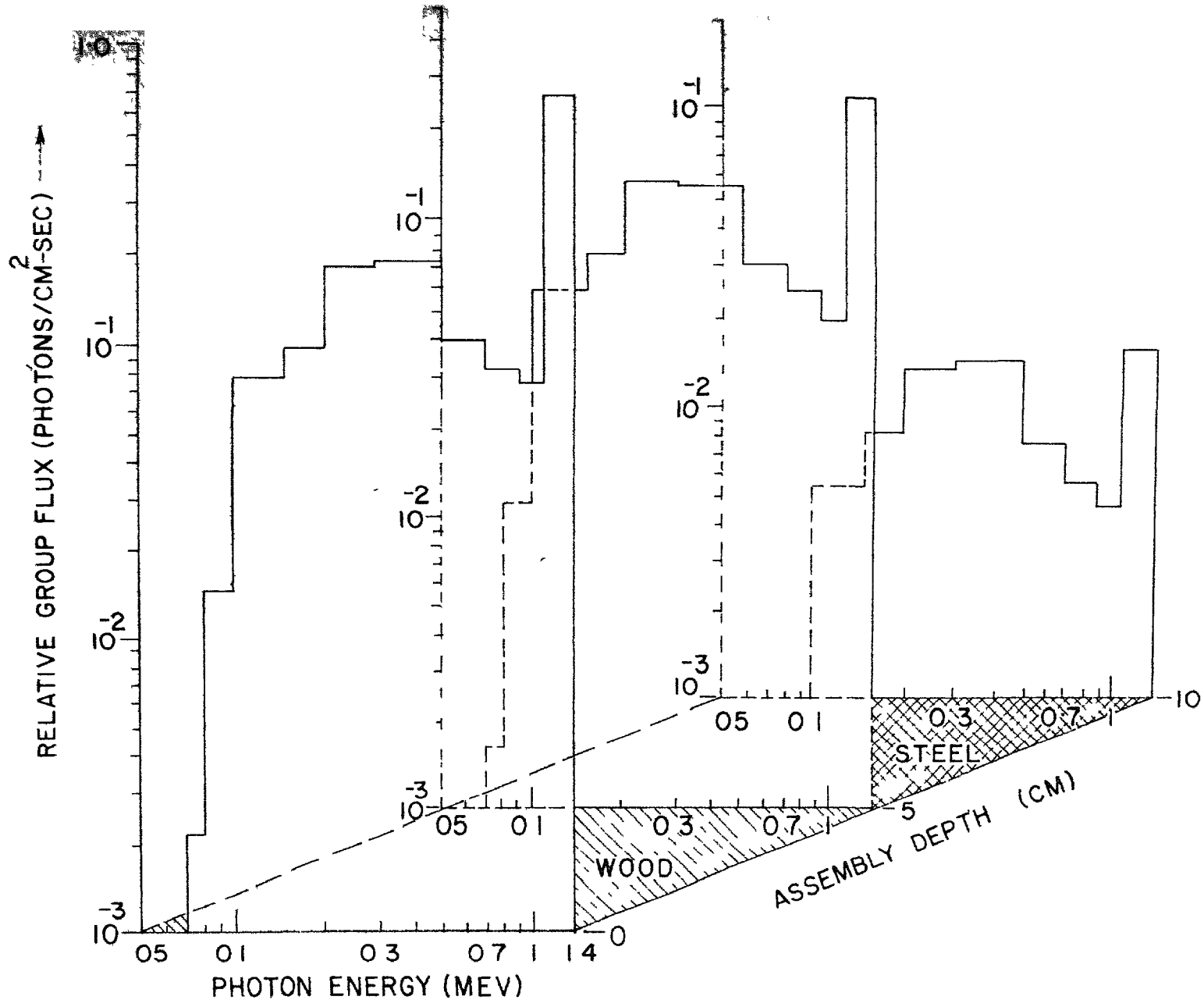

FIG. 53 ANISN-CALCULATED GAMMA-SPECTRA AT VARIOUS DEPTHS IN THE STEEL ASSEMBLY.

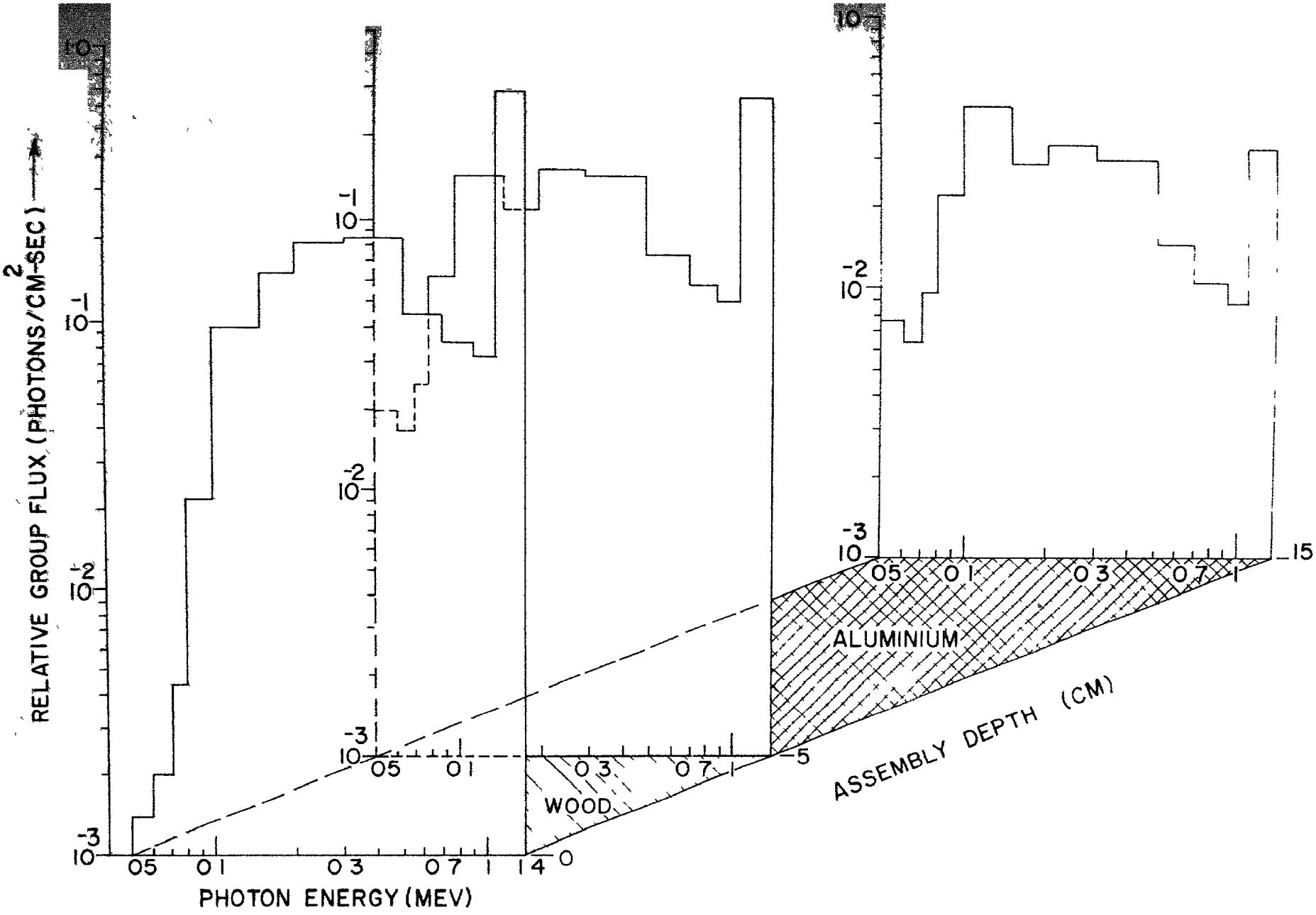

FIG 5·4 ANISN - CALCULATED GAMMA-SPECTRA AT VARIOUS DEPTHS IN THE AL ASSEMBLY

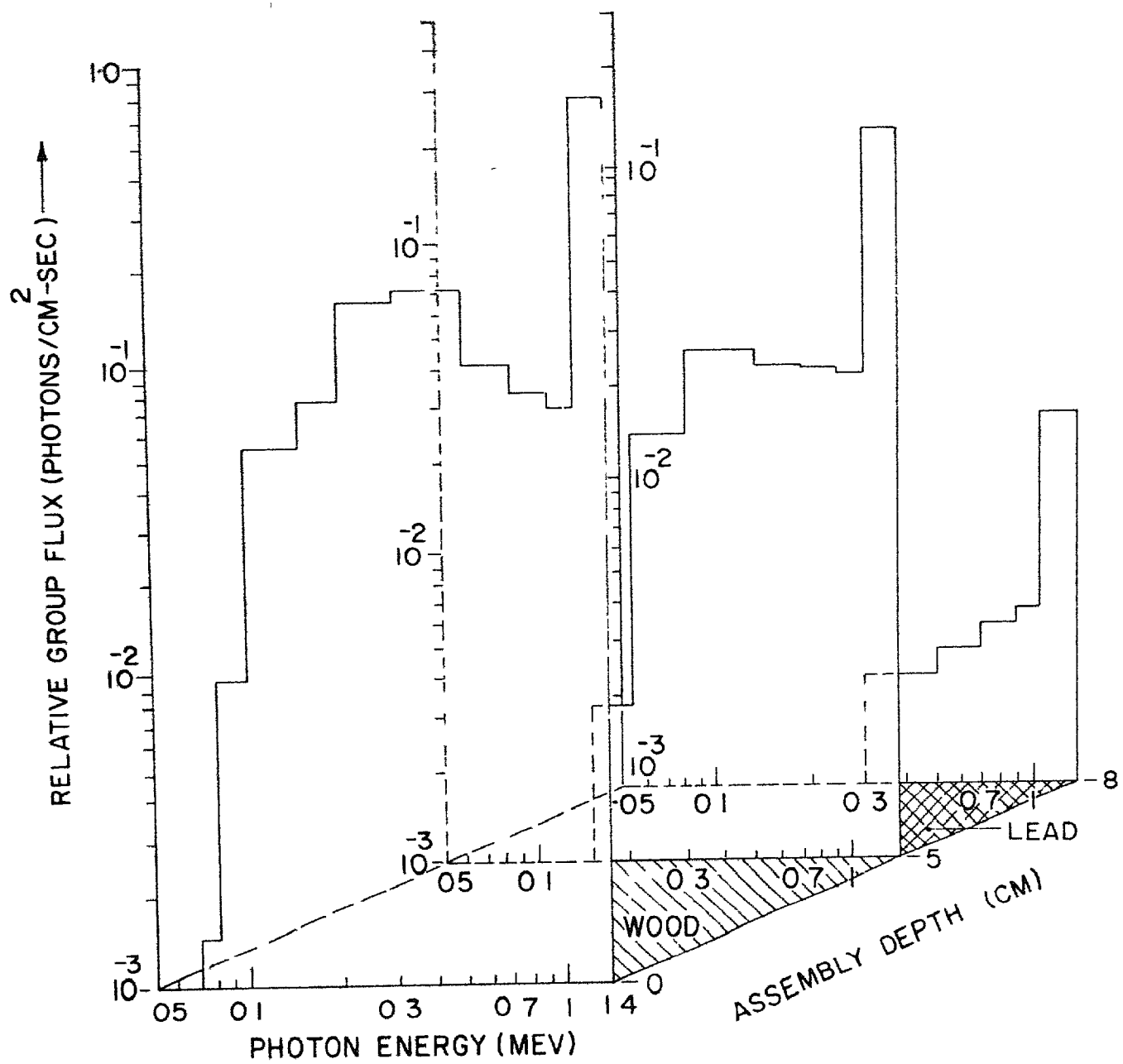

FIG.5·5 ANISN-CALCULATED GAMMA-SPECTRA AT VARIOUS DEPTHS IN THE LEAD ASSEMBLY

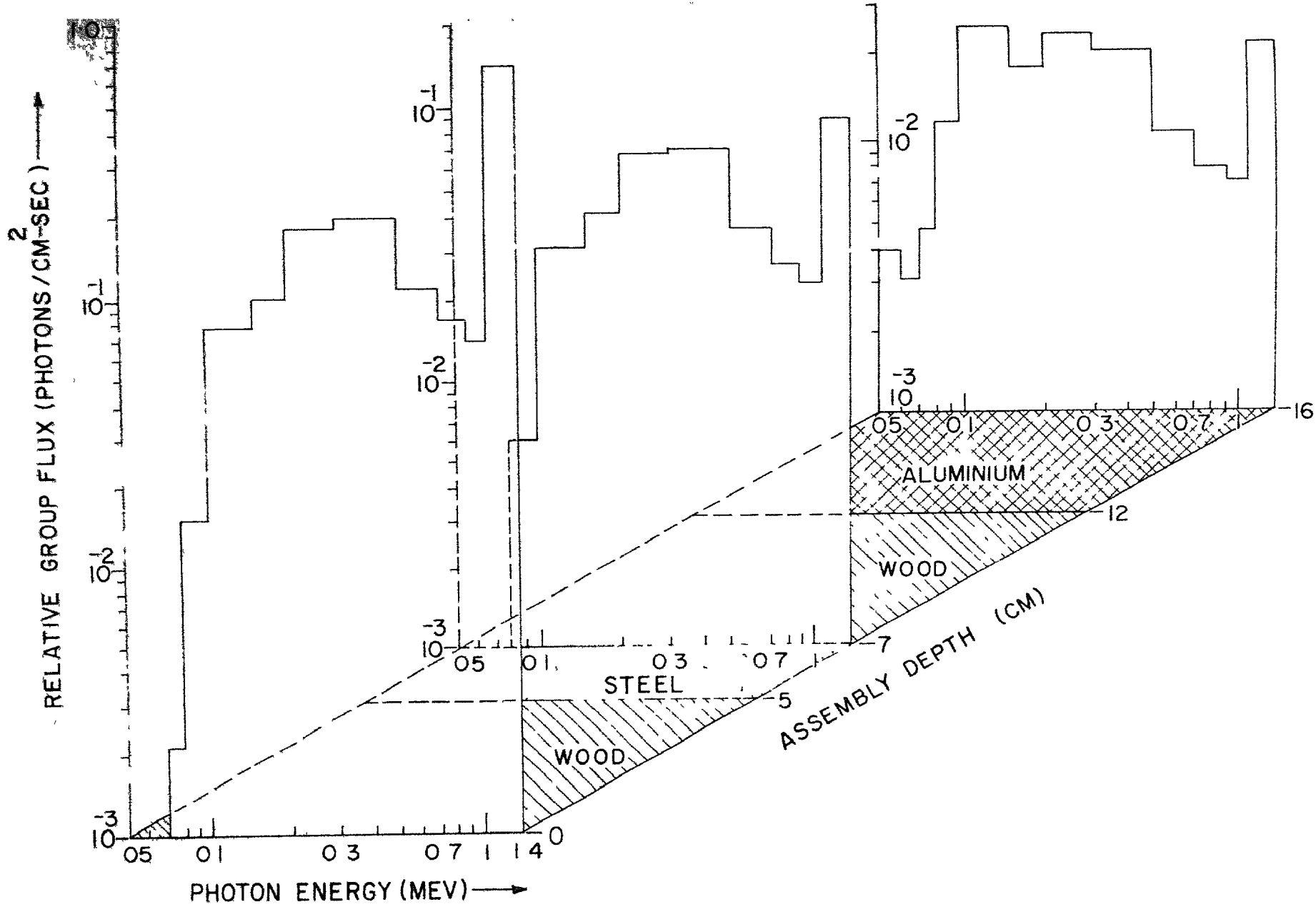

FIG.5·6 ANISN-CALCULATED GAMMA-SPECTRA AT VARIOUS DEPTHS IN THE COMBINATION-I

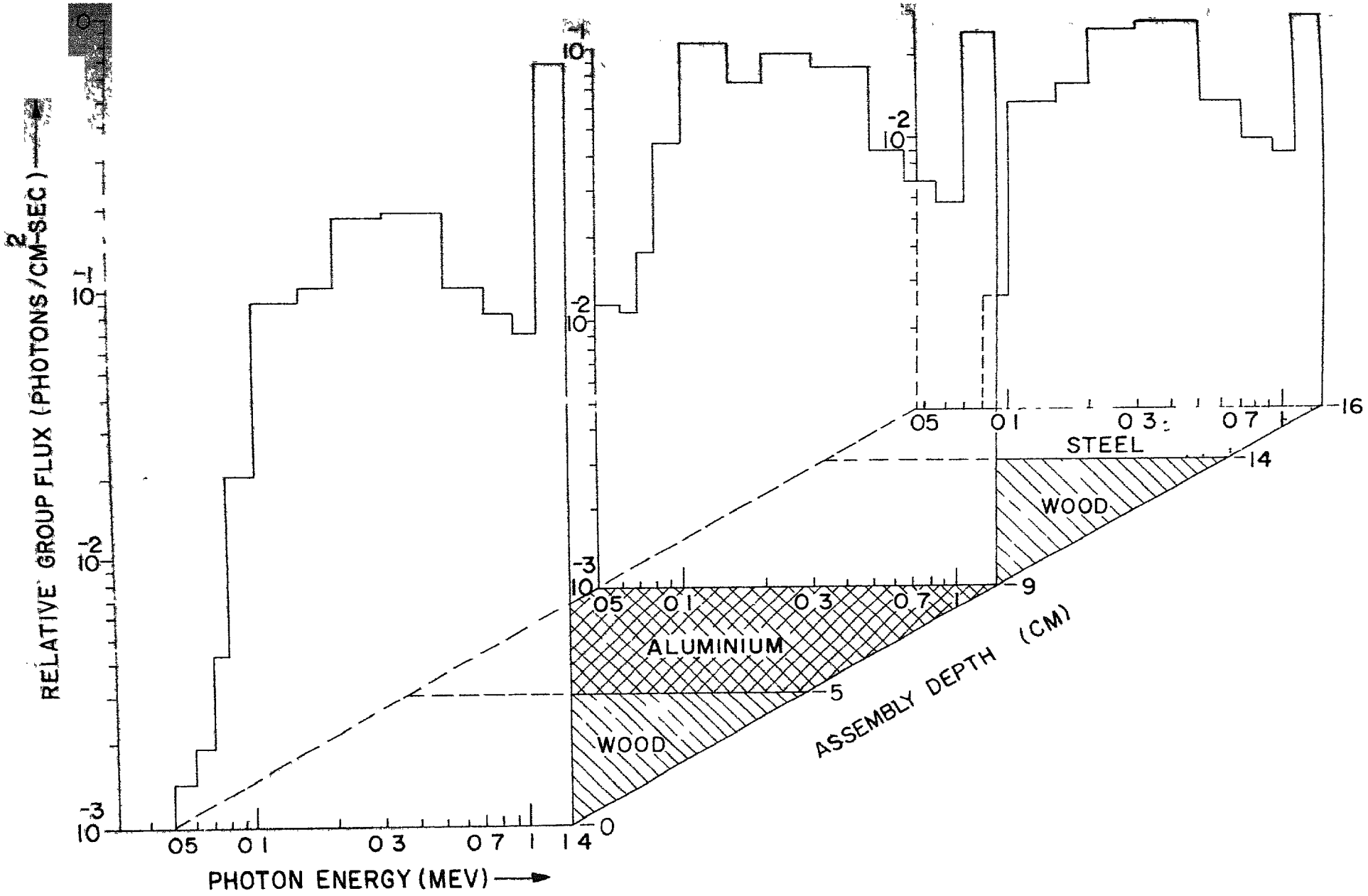

FIG 5·7 ANISN-CALCULATED GAMMA-SPECTRA AT VARIOUS DEPTHS IN THE COMBINATION-2

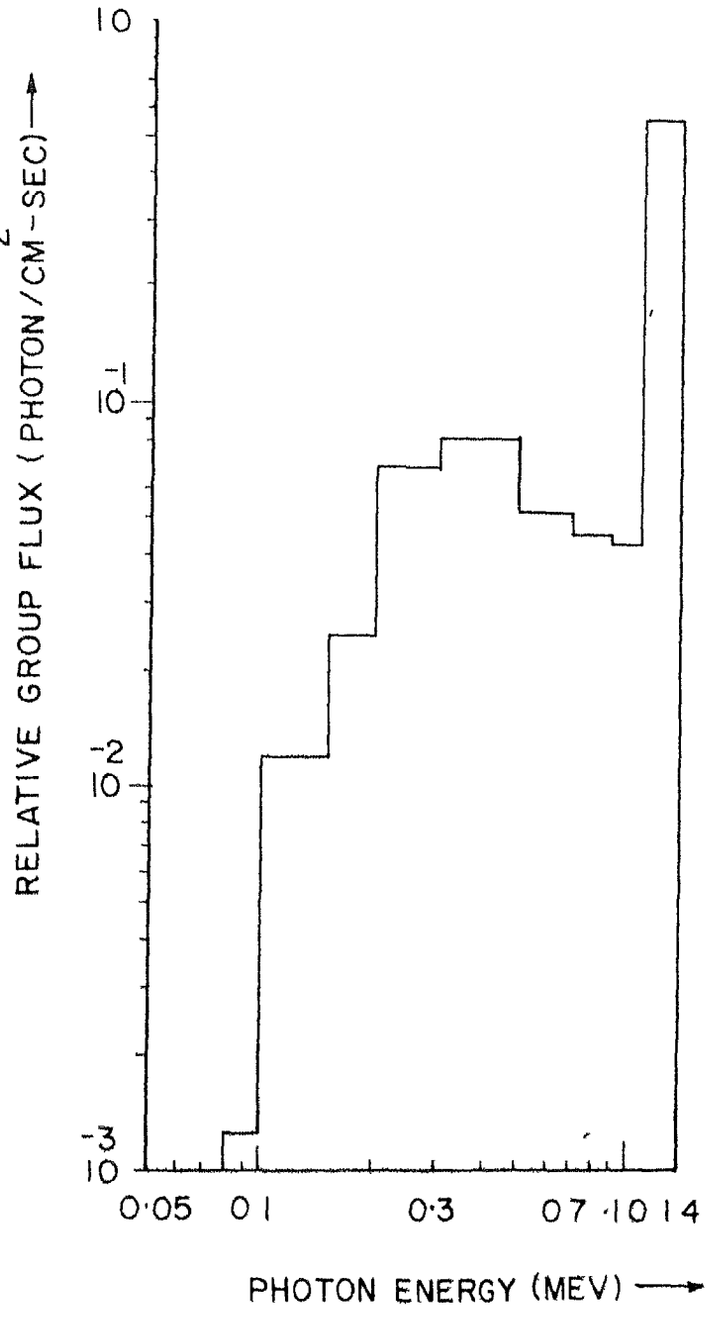

FIG. 5·7 (a) ANISN-CALCULATED SPECTRUM OF EMERGENT γ-RAYS FROM THE FIPLY SOURCE.

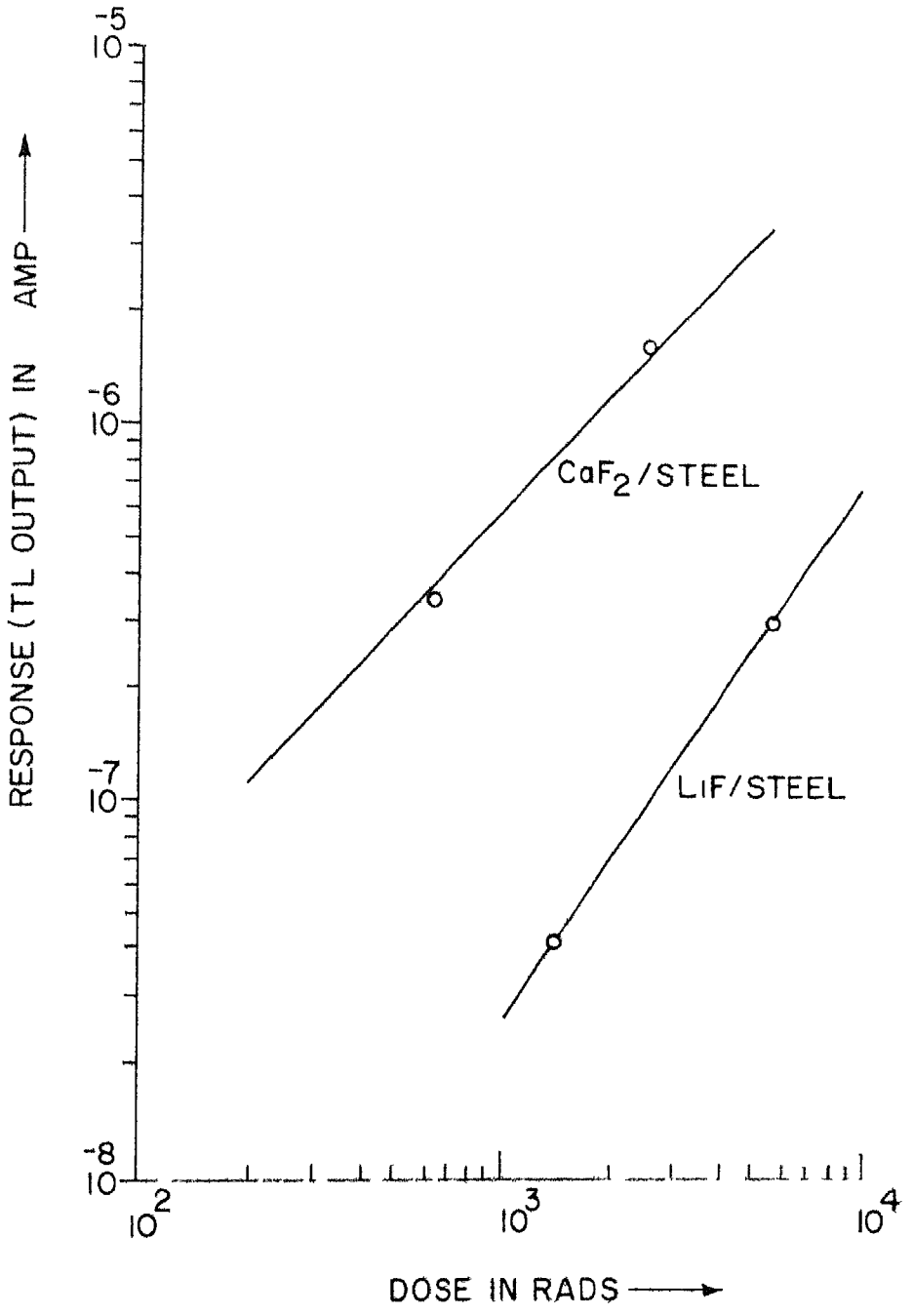

FIG. 5·8 TYPICAL RESPONSE VS. DOSE CURVES FOR LiF AND CaF_2 TLD'S.

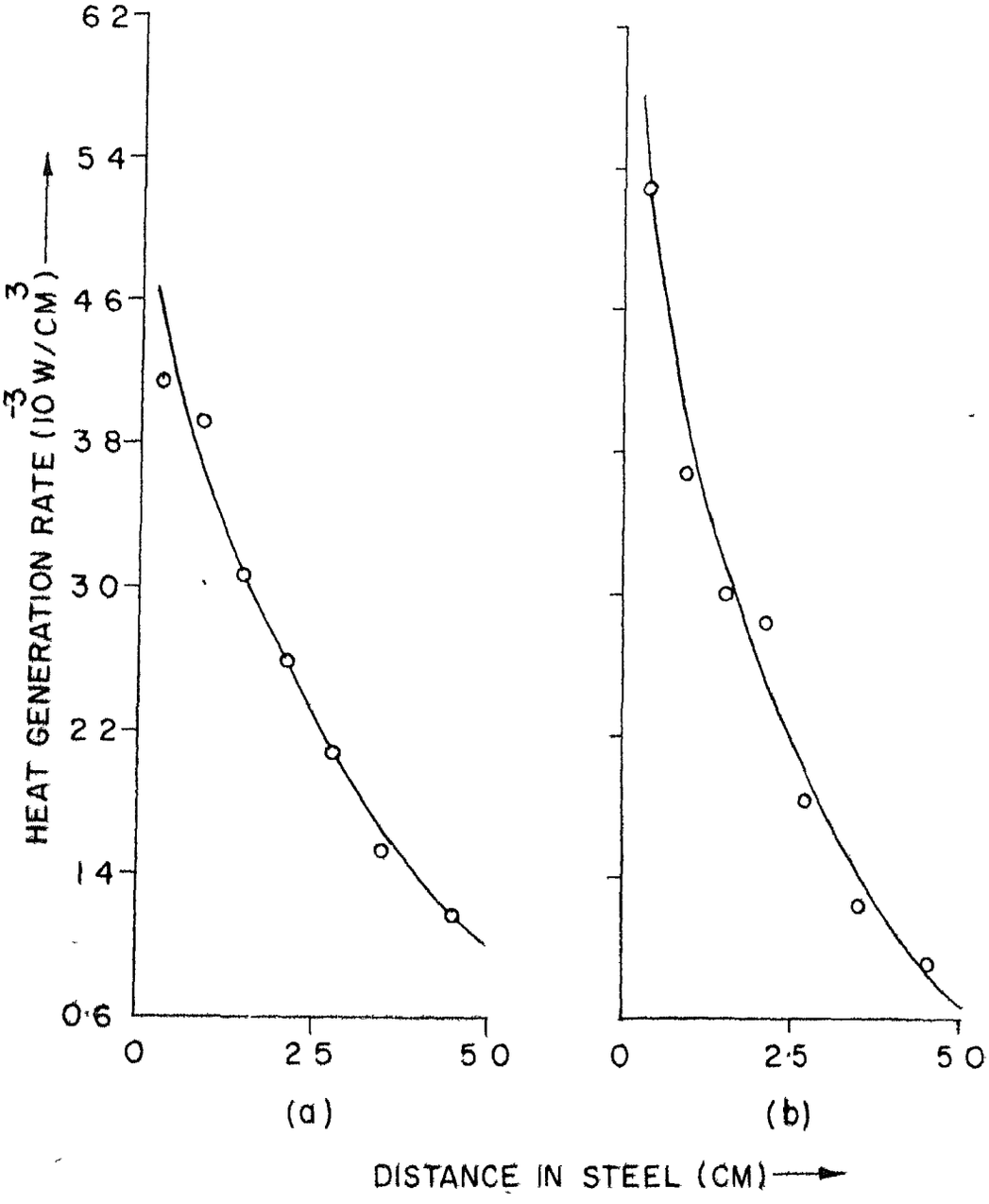

FIG 5·9 HEAT GENERATION RATES IN THE STEEL PLATES OF THE STEEL ASSY. MEASURED USING (a) CaF_2 (b) LiF

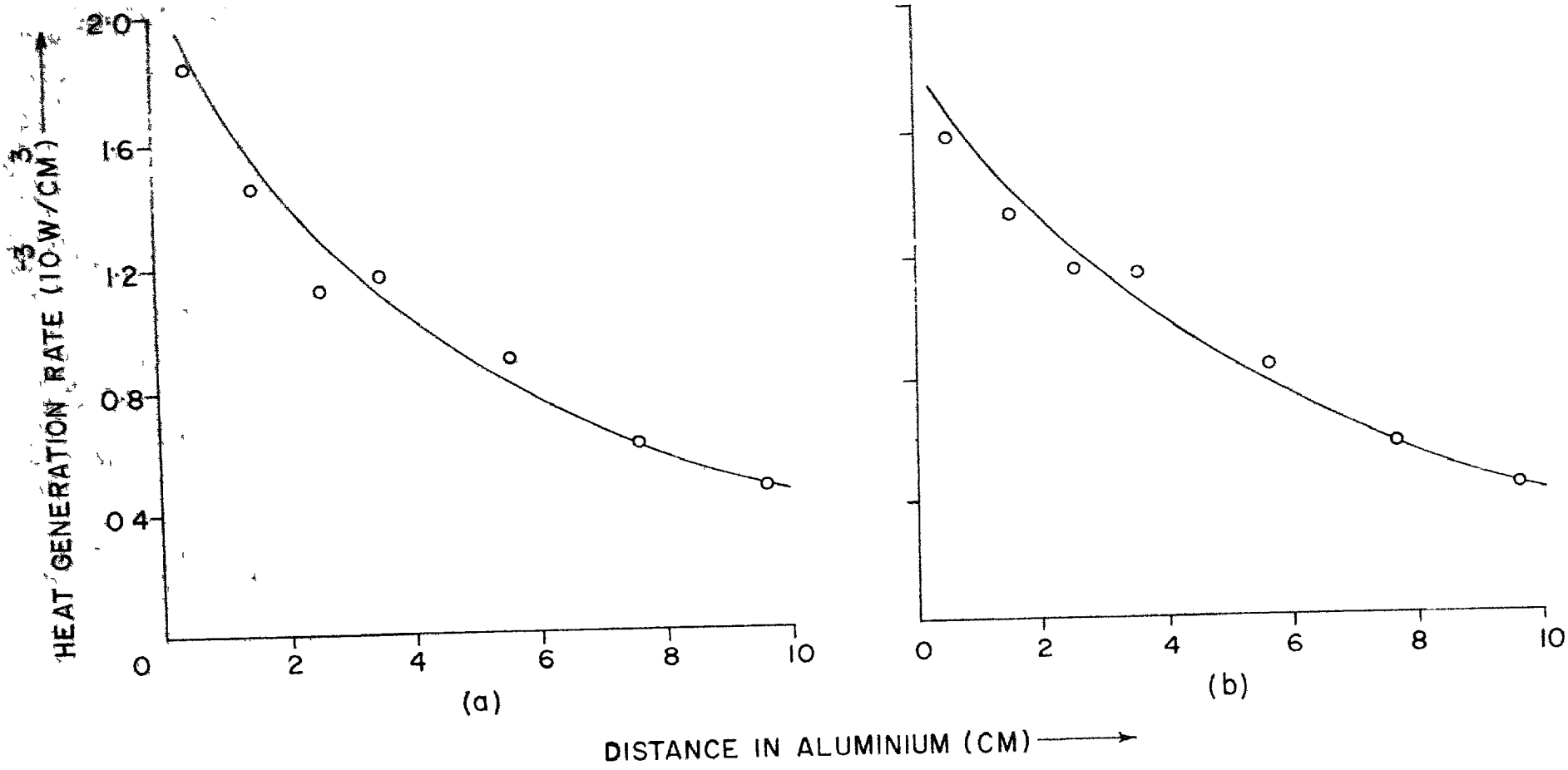

FIG.5·10 HEAT GENERATION RATES IN THE ALUMINIUM PLATES OF THE ALUMINIUM ASSEMBLY MEASURED USING (a) CaF_2 (b) LiF

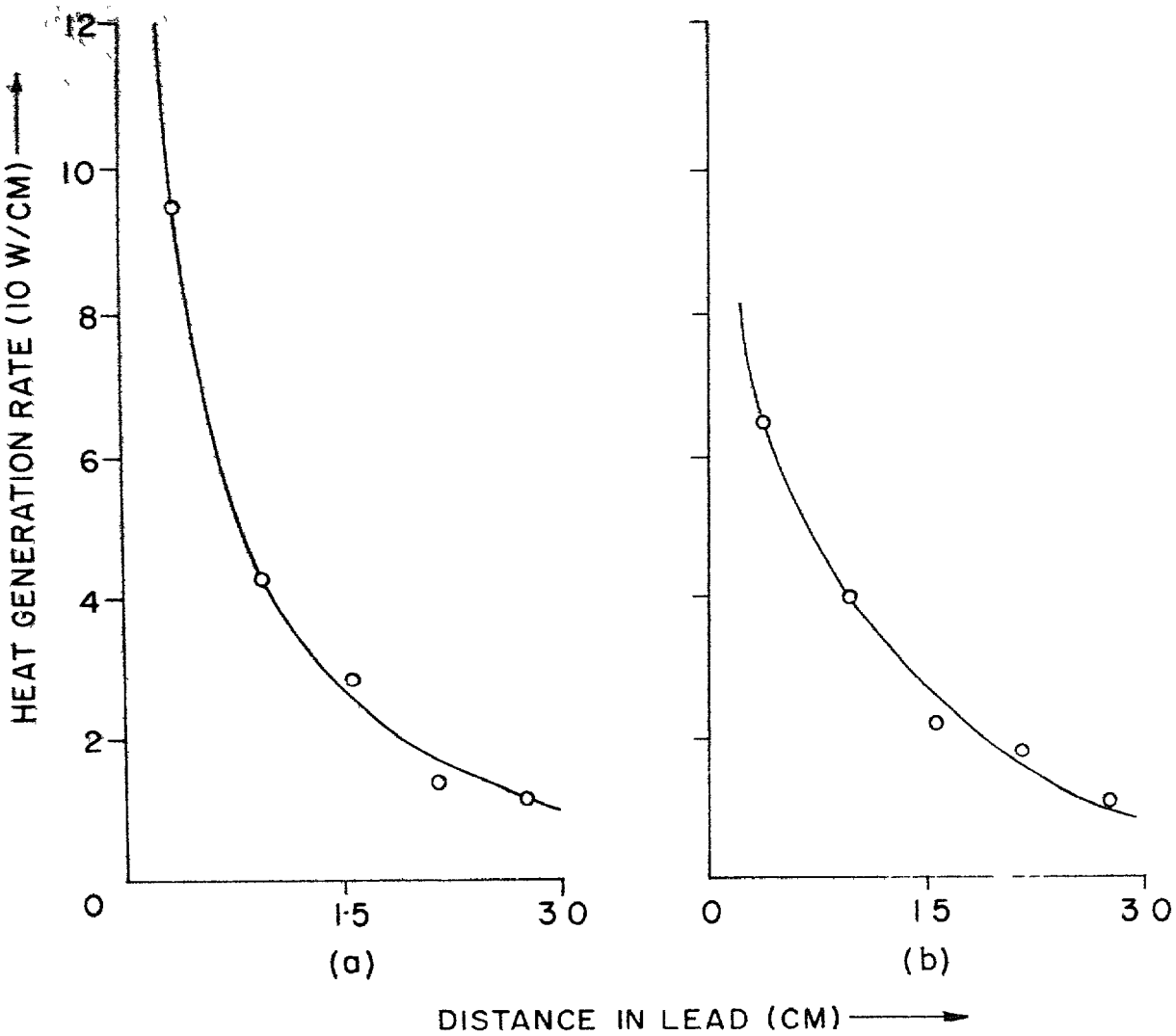

FIG.5·11 HEAT GENERATION RATES IN THE LEAD PLATES OF THE LEAD ASSEMBLY MEASURED USING (a) CaF_2 (b) LiF

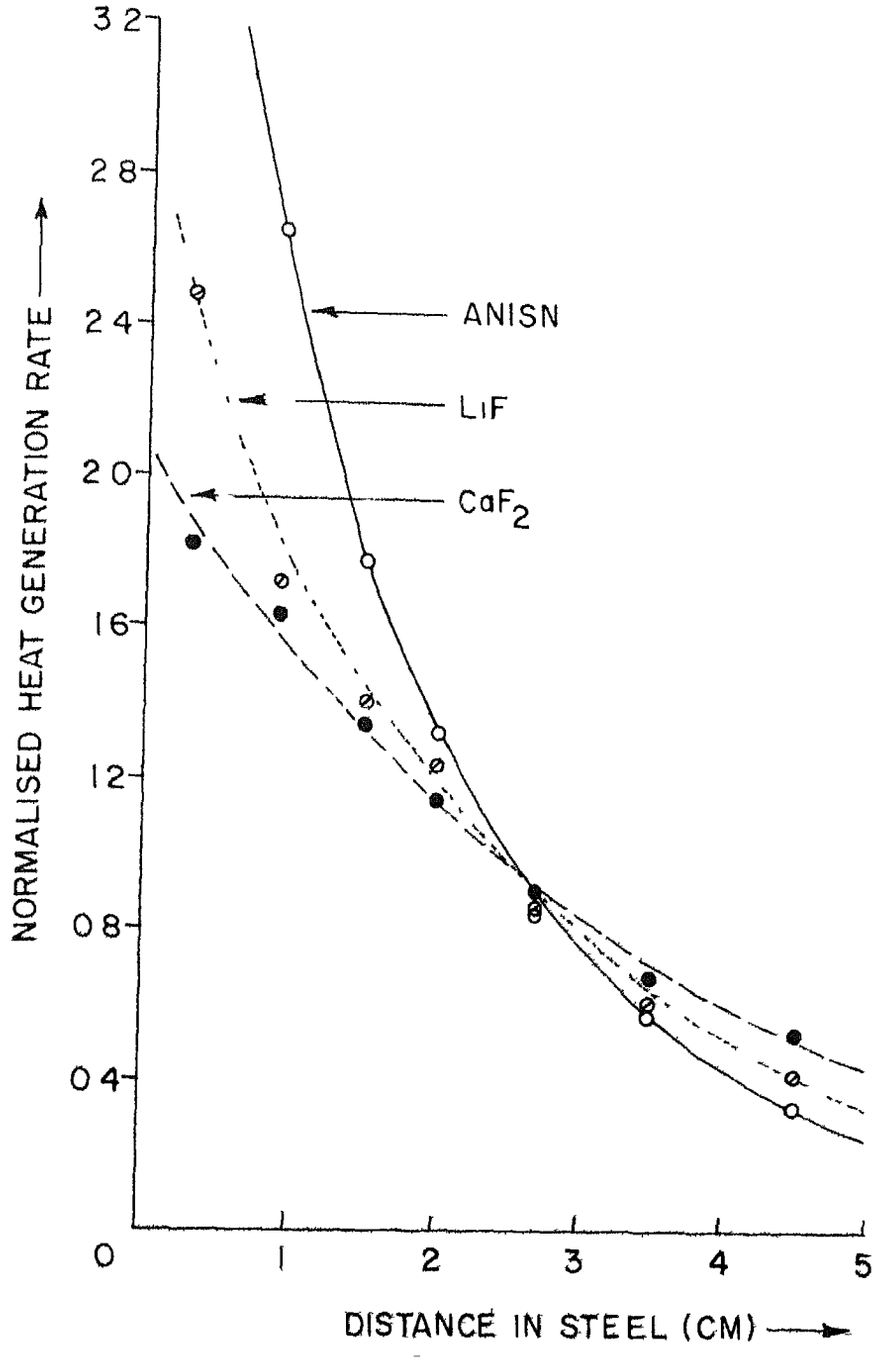

FIG. 5·12 COMPARISON OF NORMALISED MEASURED & ANISN—CALCULATED GAMMA-HEATING RATES IN THE STEEL PLATES OF THE STEEL ASSEMBLY.

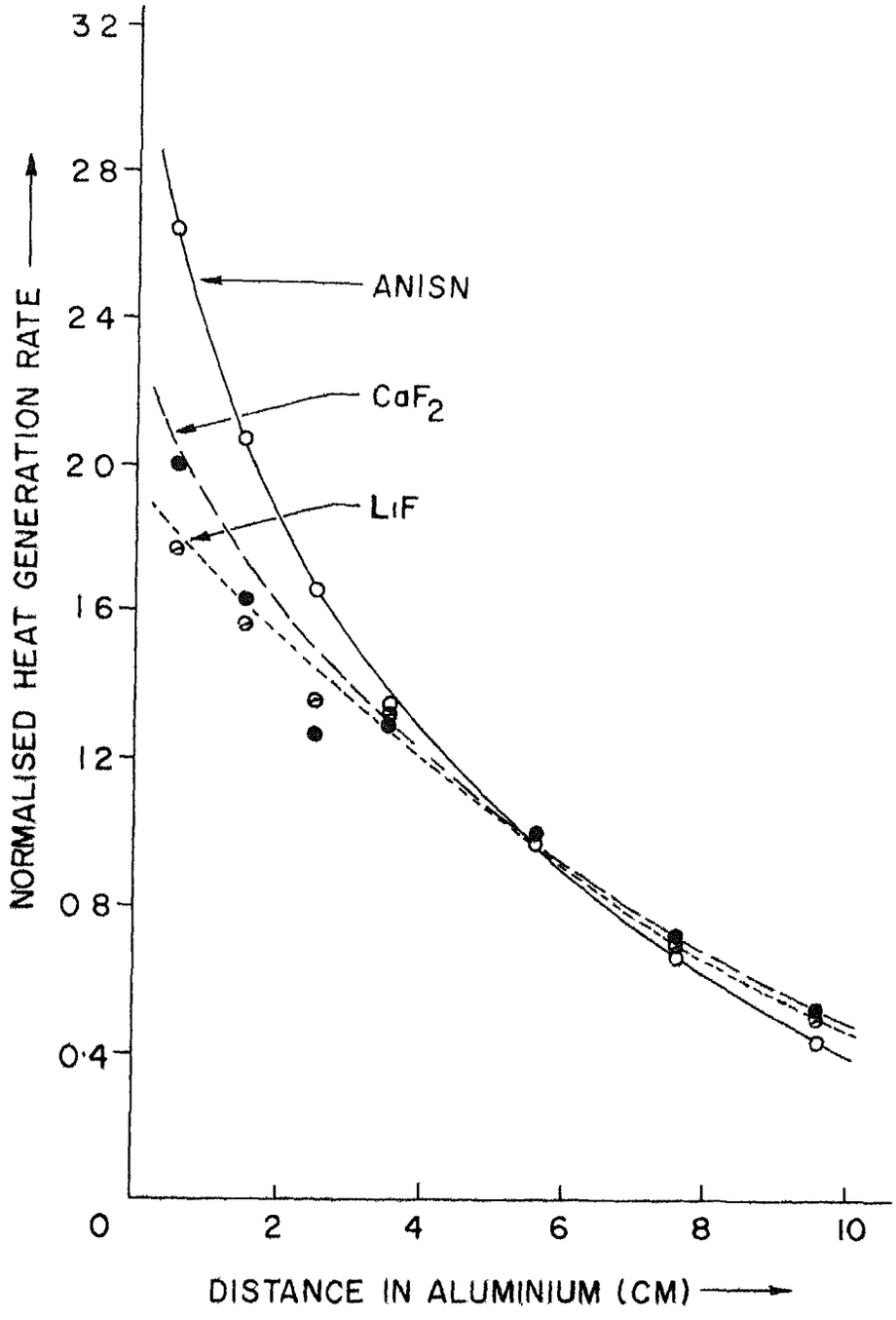

FIG. 5·13 COMPARISON OF NORMALISED MEASURED & ANISN CALCULATED GAMMA HEATING RATES IN THE AL. PLATES OF THE ALUMINIUM ASSEMBLY.

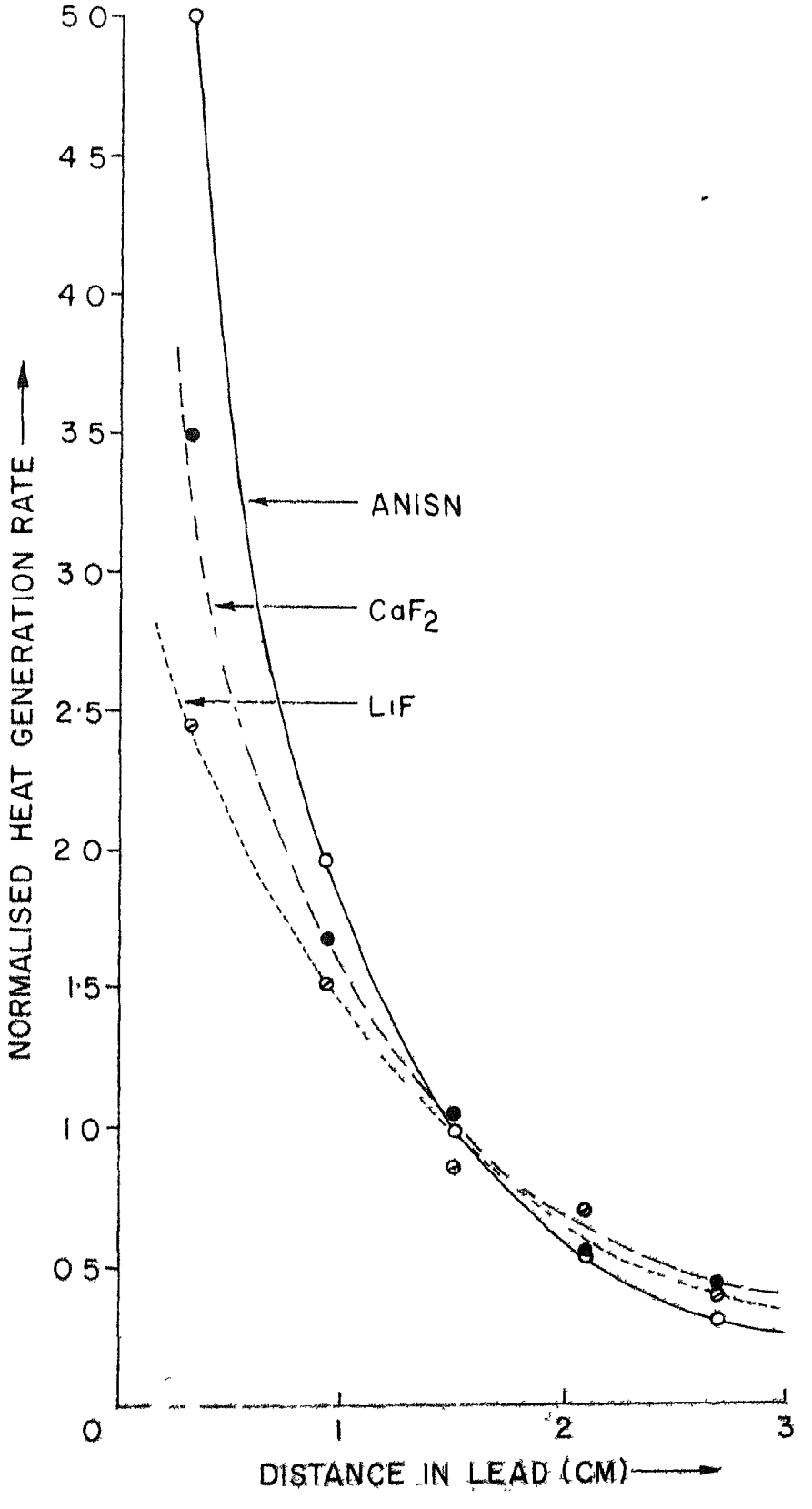

FIG.5·14 COMPARISON OF NORMALISED MEASURED & ANISN CALCULATED γ HEATING RATES IN THE LEAD PLS OF THE LEAD ASSY.

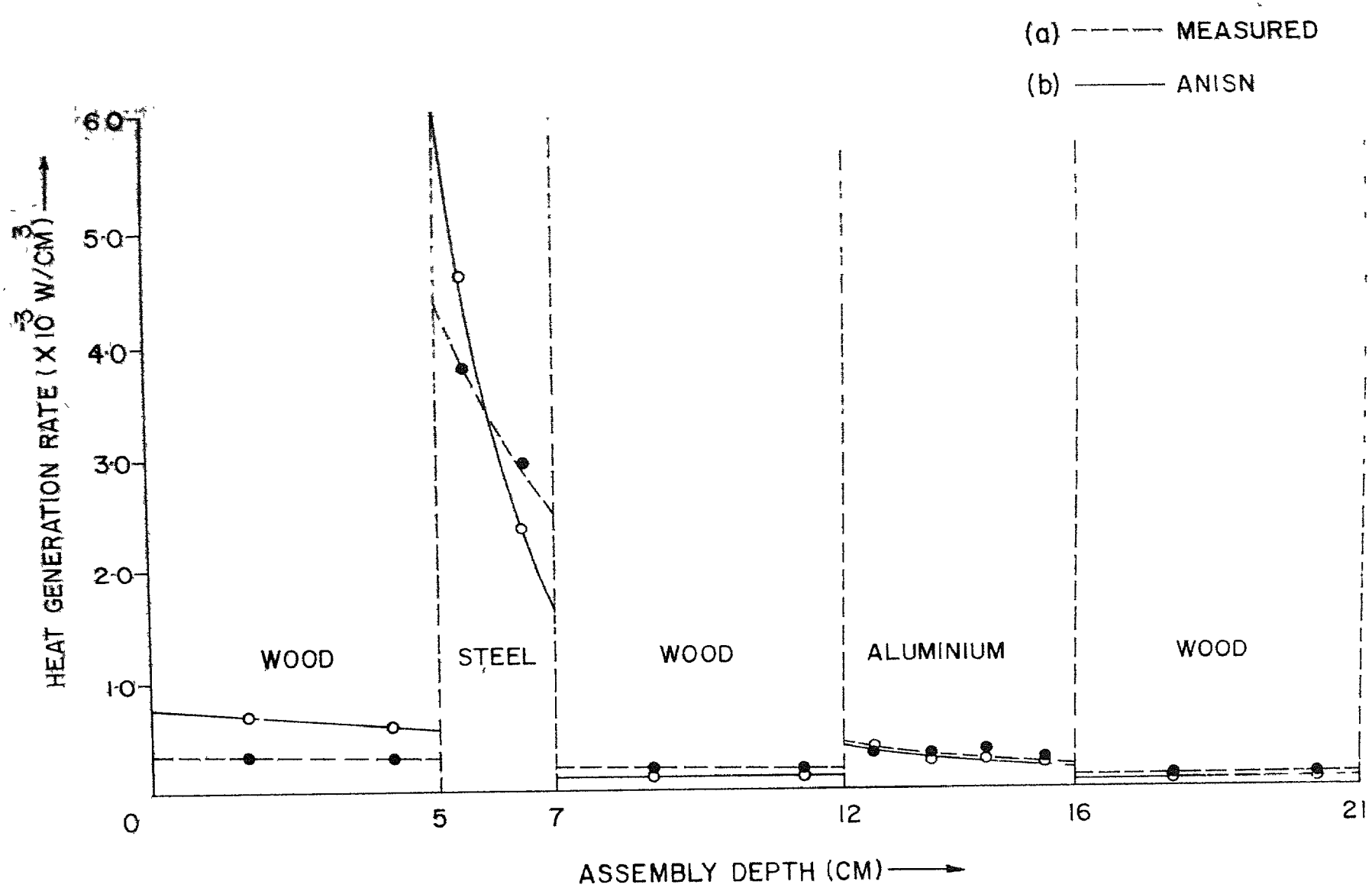

FIG. 5 15 HEAT GENERATION RATES IN THE VARIOUS PLATES OF COMBINATION-I
(a) MEASURED USING CaF_2 (b) ANISN NORMALISED TO CENTRE OF STEEL

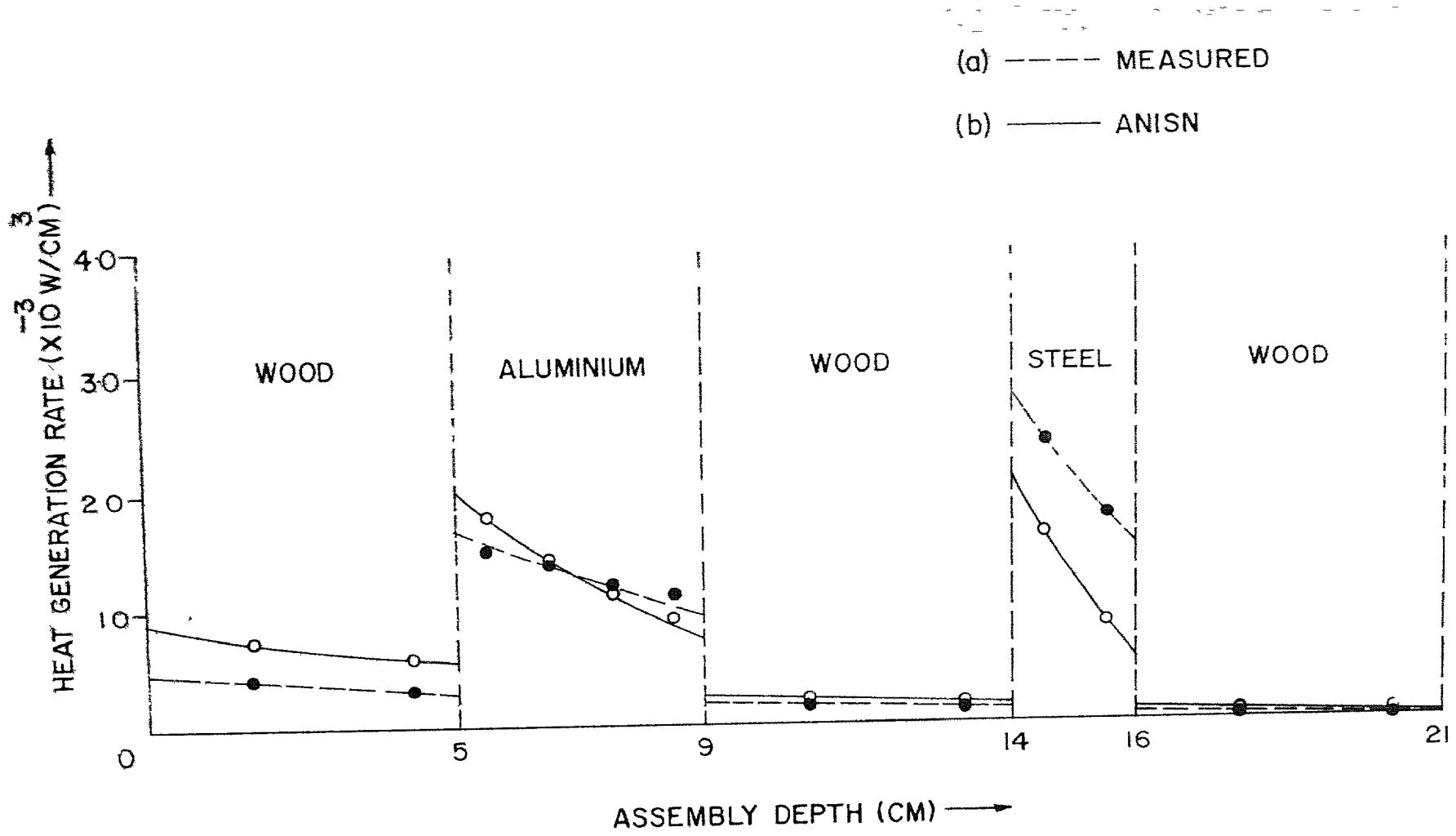

FIG. 5·16 HEAT GENERATION RATES IN THE VARIOUS PLATES OF COMBINATION–2

(a) MEASURED USING CaF_2 (b) ANISN NORMLISED TO CENTRE OF ALUMINIUM

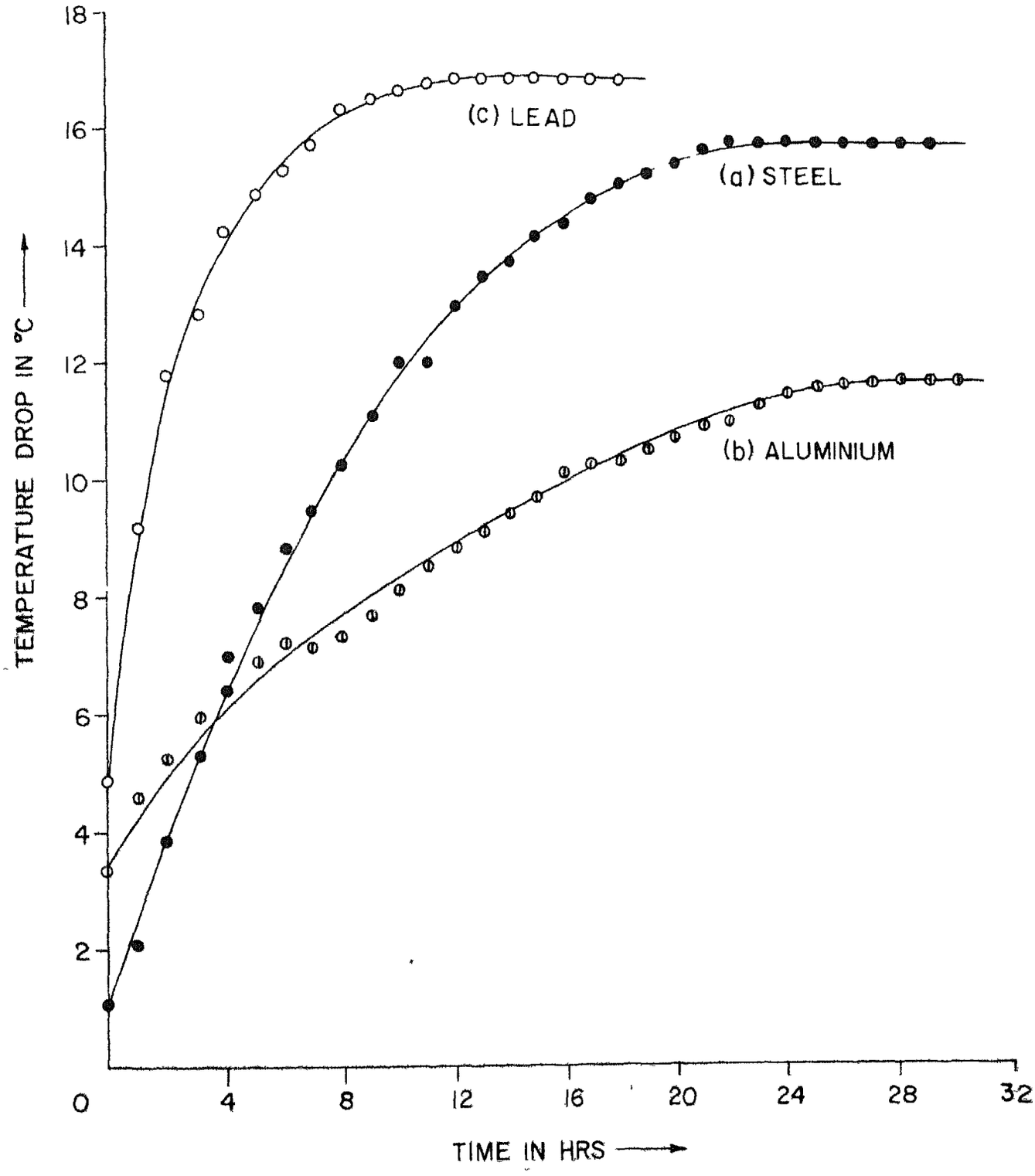

FIG.5·17 ΔT_1 TRANSIENTS FOR (a) STEEL, (b) AL. (c) LEAD ASSYS.

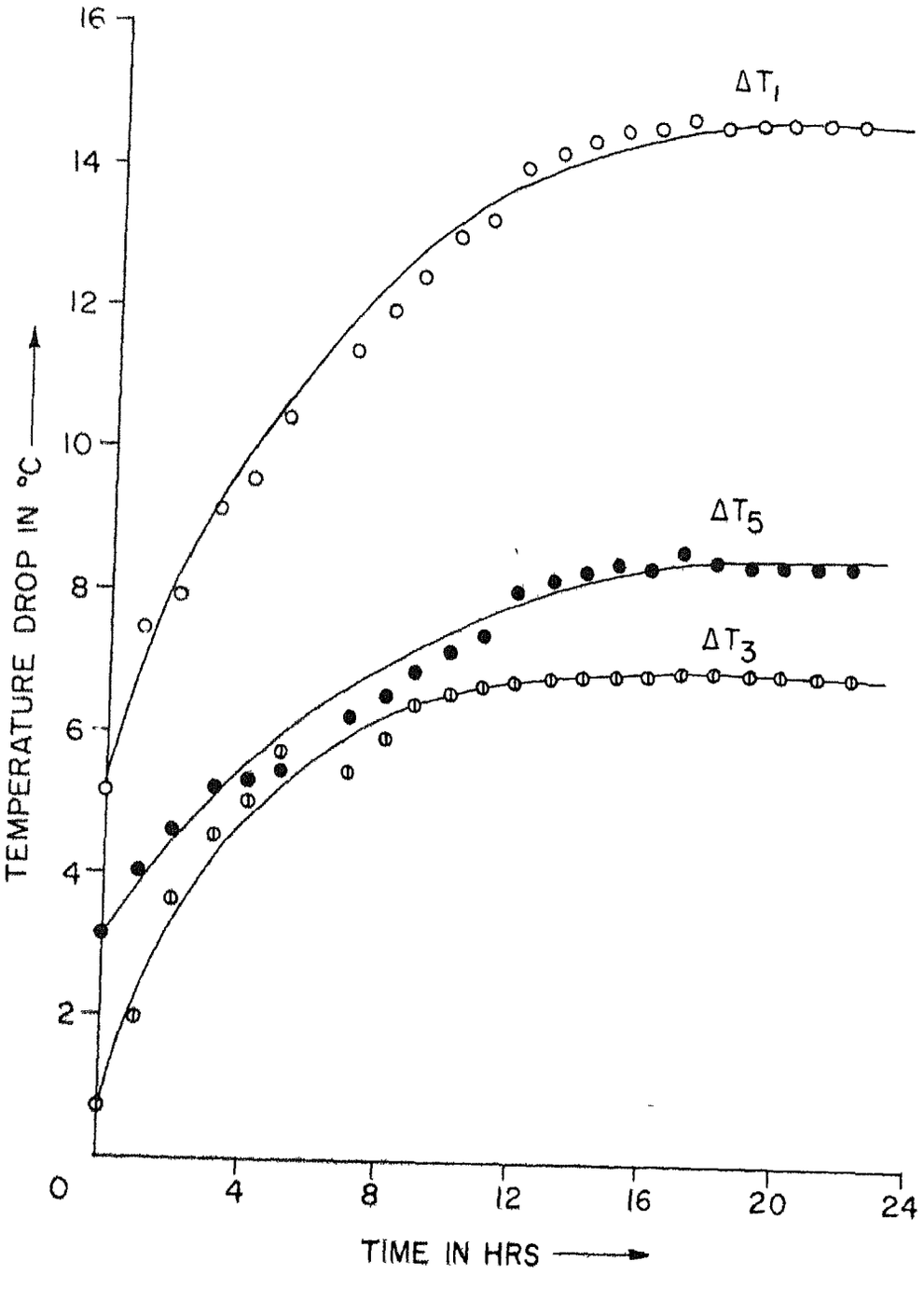

FIG. 5·18 ΔT_1, ΔT_3, ΔT_5 TRANSIENTS FOR COMBINATION-I

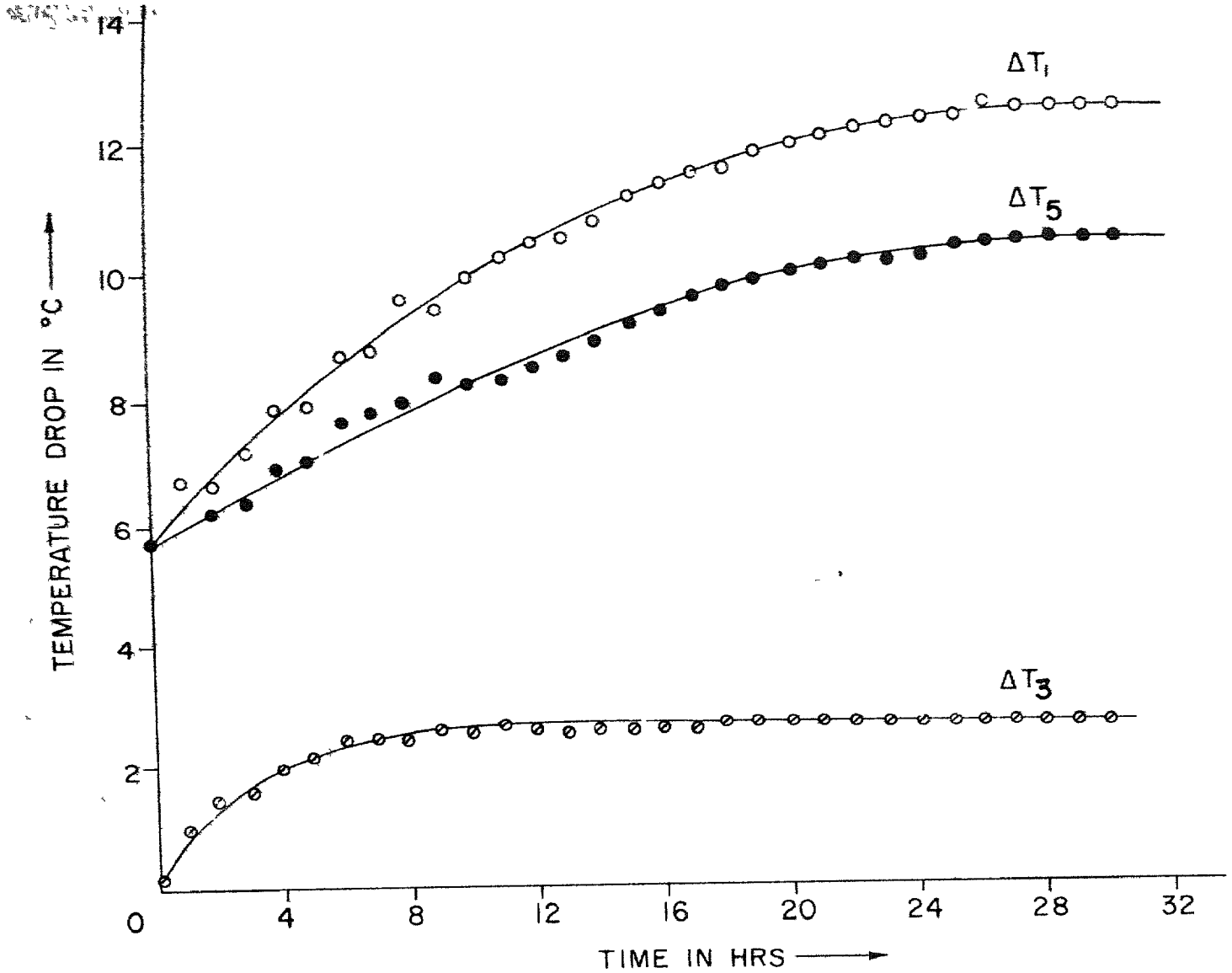

FIG. 5.19 $\Delta T_1, \Delta T_3, \Delta T_5$ TRANSIENTS FOR COMBINATION-2

CHAPTER 6

CONCLUSIONS AND SCOPE FOR FURTHER WORK

6.1 CONCLUSIONS

The use of TLD's for carrying out gamma-heating measurements in several reactor materials has been assessed through temperature measurements across specially-designed assemblies. Thus, in effect, a direct comparison of dosimetric and calorimetric techniques for gamma-heating evaluation has been shown possible. The materials considered presently were steel, aluminium, lead and wood.

The accuracy of gamma-heating determinations by the TLD technique is limited by uncertainties in the gamma-spectrum-dependent relationship between energy deposited in the dosimeter and that in the surrounding material (the $\frac{1}{f}$ - factor). The better the matching in effective atomic number between the dosimeter and surrounding material, the less is the uncertainty. Cobalt-60 gamma spectra within the experimental assemblies in the present study were estimated from infinite-slab-geometry calculations with the ANISN code. Adequacy of the calculated $\frac{1}{f}$ - factors was, however, established by obtaining reasonable agreement in energy-deposition rates deduced using LiF and CaF_2 TLD's (with effective atomic numbers of 8.2 and 16.3, respectively).

With the TLD-measured heat-generation rates fed as input, steady-state temperature drops across the low-conductivity material, wood, in the various assemblies were deduced from the three-dimensional heat-conduction code, HEATING. These were compared with actual thermocouple measurements. The agreement obtained was within about 5% in most cases, i.e. quite consistent with errors of ± 5% systematic and ± 3% random, as assessed for a typical experiment.

6.2 SCOPE FOR FURTHER WORK

The present study has been carried out using a large cobalt-60 source for irradiation. It would be instructive to carry out experiments of the present type in a reactor environment, so that

(i) a more characteristic gamma-ray spectrum is considered for assessing the adequacy of gamma-heating measurements with TLD's and

(ii) the accuracy of corrections for the neutron sensitivity of the TLD's may also be assessed.

Accurate estimation of gamma spectra (particularly the low-energy component) would be essential for evaluating appropriate $\frac{1}{f}$ - factors. Theoretical estimates could be supported by experimental measurements,

e.g. the comparison of the TLD response, in both the reactor and the calibration facility, with ion-current chamber measurements (3).

For minimal neutron sensitivity, a higher effective atomic number for the TLD would probably be better because of the lower average energy of the recoil ions produced in elastic scattering. The preference of CaF_2 over ^{7}LiF for gamma-heating measurements thus becomes even more justified in a reactor environment. (^{6}LiF would, of course, not be usable because of its high neutron absorption cross-section).

REFERENCES

1. Attix, F.H., and Roesch, W.C., "Radiation Dosimetry", 2nd ed., Vol. II, Academic Press, New York, (1966).

2. Cameron, J.R., Suntharalingam, N., Kenney, G.N., "Thermoluminescent Dosimetry", The University of Wisconsin Press, Madison, Wisconsin (1968).

3. Stanford, G.S., and Johnson, T.W., "Determination of Gamma-ray Heating in a Critical Facility by Thermoluminescent Dosimetry", Report No. ANL-7373 (1968).

4. Adamson, J., et. al., "ZEBRA-6 Dilute Plutonium Fuelled Assembly", Report No. ANL-7320 (1966).

5. Boulette, E.T., and Bunch, W.L., "Analysis of ZPPR/FTR Shield Experiments - Gamma Distributions", Report No. WHAN-FR-13 (1971).

6. Stanford, G.S., et. al., "Gamma-ray Heating by Thermoluminescent Dosimetry in the FTR Engineering Mockup Shielding Experiments", Report No. ANL-8010 (1973).

7. Simons, G.G., "Thermoluminescent Dosimetry Applied to Gamma-ray Dose Measurements in Critical Assemblies", Report No. ANL-7710 (1971).

8. Simons, G.G., and Olson, A.P., "Analysis and Measurements of Gamma-ray Heating in the Demonstration Benchmark Plutonium Fuelled Critical Assembly", Nuclear Science and Engineering, 53, 176 (1974).

9. Price, C.C., Laskiewicz, R.A., and Lowery, V.W., "A Passive Calorimetry System for Measuring Gamma Energy Deposition Rates in an LMFBR", Trans. Am. Nucl. Soc., 22, 684 (1975).

10. Reilly, H.J. and Peters, L.E., "Calorimetric Determination of Relative Gamma Heating in Materials of Various Thicknesses and Atomic Numbers", Nuclear Technology, 11, 89 (1971).

11. Meklveen, J. W. and Schwenk, M., "Reactor Flux Measurements Using Thermoluminescent Dosimetry", Nuclear Technology, 31, 257 (1976).

12. Burlin, T.E., "Cavity-Chamber Theory", Radiation Dosimetry, 2nd 2d., Vol. 1, Chapter 8, Academic Press, New York (1968).

13. Burlin, T.E., "A General Theory of Cavity Ionization", British Journal of Radiology, 39, 727 (1966).

14. Tochilin, E., "Thermoluminescent Dosimetry for Shielding Studies in a Reactor Environment", Trans. Am. Nuclear Soc., 13, 420 (1970).

15. Busuoli, G., and Cavallini, A., Private Communication.

16. Oltman, B.G., et. al., "The Effects of Fast Neutrons Exposure on ^{7}LiF Thermoluminescence Response to Gamma-rays", Health Physics, 13, 918 (1967).

17. Goldstein, N., Miller, W.G. and Rago, P.F., "Additivity of Neutron and Gamma-ray Exposures for TLD Dosimeters", Health Physics, 18, 157 (1970).

18. Simons, G.G., and Yule, T.J., "Gamma-ray Heating Measurements in Zero Power Fast Reactor with TLD's", Nuclear Science and Engineering, 53, 162 (1974).

19. Puite, K.J., "Thermoluminescent Sensitivity of CaF_2:Mn in a Mixed Neutron-Gamma Field", Health Physics, 20, 437 (1971).

20. Soltesz, R.G., et. al., "One Dimensional Discrete Transport Technique", Report No. WANL-PR(LL)-034, Vol. 4, (1970).

21. Engle, W.W., Jr., "A User's Manual for ANISN - A One Dimensional Discrete Ordinates Transport Code with Anisotropic Scattering", Report No. K-1693 (1967).

22. Carlson, B.G., "A Review of the Discrete Ordinates S_n Method for Radiation Transport Calculation", Report No. ORNL-RSIC-19 (1968).

23. Hubbell, J.H., "Photon Cross-sections, Attenuation Coefficients and Energy Absorption Coefficients from 10 KeV to 100 GeV", Report No. NSRDS-NBS-29 (1969).

24. Jaeger, R.G., et. al., "Engineering Compendium on Radiation Shielding, Vol. 1", Springer-Verlag, New York (1968).

25. Sastry, S.R., "HEATING - A Computer Program for the Solution of Generalized Heat Conduction Equations", Internal Report, B.A.R.C., Trombay (1972).

26. Fowler, T.B., and Volk, E.R., "Generalized Heat Conduction Code for the IBM-704 Computer", Report No. ORNL-2734 (1959).

27. "Instruction Manual Cobalt-60 Irradiator Type IRII", A.E.E., Trombay (1966).

28. Rao, P.S., Govindarajan, K.N., and Gupta, U.C., "Indirect Intercomparison of Exposure Standards", Report No. BARC-762 (1974).

29. Berger, M.J. and Seltzer, S.M., "Tables of Energy Losses and Ranges of Electrons and Positrons", Report No. NASA-SP-3012 (1964).

30. Berger, M.J. and Seltzer, S.M., "Additional Stopping Power and Range Tables for Protons, Mesons and Electrons", Report No. NASA-SP-3036 (1966).

31. Brady, G.S., "Materials Handbook", 8th Edition, McGraw-Hill, New York (1956).

32. Dassi, P., Busuoli, G., and Rimondi, C.,"Calculated Energy Dependence of Some RTL and RPL Detectors", International Journal of Applied Radiation and Isotopes, 27, 291 (1976).

33. Visser, C.J. and Mouton, W.L., "The Energy Spectrum of a Relatively Large Kilocurie ^{60}Co Source Used in Agriculture", International Journal of Applied Radiation and Isotopes, 26, 573 (1975).

34. Raznjevic, K., "Handbook of Thermodynamic Tables and Charts", 1st Edition, McGraw-Hill, New York (1976).

35. Perry, J.H., "Chemical Engineer's Handbook", 4th Edition, McGraw-Hill, New York (1963).

36. "Product Specifications", M/s Mettur Beardsell Ltd. (Thermocole Manufacturers), Bombay (1977).

NETP - 1978 - M - DHA - 0555